The Convective Mantle Flow Signal in Rates of True Polar Wander

Bernhard Steinberger

Institut für Meteorologie und Geophysik, Johann Wolfgang Goethe-Universität, Frankfurt am Main, Germany

Richard J. O'Connell

Department of Earth and Planetary Sciences, Harvard University, Cambridge, Massachusetts

We investigate changes of the rotation axis caused by mantle convection. In the first part, the coupled problem of viscoelastic deformation and rotational dynamics is solved for simple Earth models in order to compute how the rotation axis changes following emplacement of non-hydrostatic excess masses. It is shown that both direct integration and a computationally more effective "quasi-static integration" give virtually identical results. With the latter method, results of eigenmode and time domain approach were compared, with little difference found. Although the number of viscoelastic relaxation eigenmodes is infinite, for an adiabatic Earth mantle only two eigenmodes need be considered for an approximately correct description, and an even simpler steady-state solution can be used. The results indicate that for our best estimates of present-day mantle properties, the maximum speed of polar motion is about 1 degree per million years, and during Cenozoic times the rotation axis has always followed closely the axis of maximum non-hydrostatic moment of inertia imposed by advection of mantle density heterogeneities. The latter was calculated for a number of tomographic models and inferred flow fields. Results indicate on average a slow motion of about 5 degrees in 60 Ma roughly towards Greenwich, which is not in conflict with paleomagnetic results. Only one of the models additionally predicted a faster motion prior to about 80 Ma in a direction similar to what is inferred from paleomagnetism.

1. INTRODUCTION

1.1. Overview

While the geodetically observed rates of polar motion [*Dickman*, 1977] are believed to be to a large part due to glacial events, the longer-term polar motion may largely be due to redistributions of masses caused by convection in the Earth's mantle [e.g., *Ricard and Sabadini*, 1990], and convection may still cause a non-negligible contribution to present-day polar wander. Here we will elaborate on this issue, and for this purpose we present a numerical model for changes of the rotation axis caused by a convecting mantle and compare results with observations of true polar wander. Some important results of this model have already been published [*Steinberger and O'Connell*, 1997]. Here we expand this work essentially in two ways: Firstly, the model of viscoelastic

Ice Sheets, Sea Level and the Dynamic Earth
Geodynamics Series 29

10.1029/029GD15

relaxation that is used to compute changes of the rotation axis following a change in the moment of inertia is introduced in more detail. In this section some of the printing errors that occurred in our previous publication will also be pointed out. We will reiterate the conclusion that normally the rotation axis follows imposed changes of the moment of inertia tensor. Secondly, although only changes of the degree two non-hydrostatic geoid cause changes in long-term Earth rotation, we will compute time change of the geoid up to higher degree. Through this additional information, we are better able to pin down which features, when advected, are most responsible for the change in nonhydrostatic moment of inertia. Furthermore, we compute time changes of the moment of inertia tensor for a greater number of tomographic models, thus corroborating the robustness of our results.

Because the Earth is not rigid, it makes sense to define the axis of rotation of a reference frame relative to an inertial frame of reference. In this work, the calculations of the "rotation axis" will without further mention always refer to "Tisserand's mean axes of the body". This reference frame is characterized by zero net rotation when integrated over the entire mantle, and will be also referred to as "mean mantle" reference frame.

When comparing our computations with observations of true polar wander, we need to bear in mind that, besides the obvious axial dipole hypothesis, the comparison also assumes that the mean mantle reference frame in which our calculations are performed and which cannot be directly constrained by observations, and the "hotspot reference frame" which is based on observations and to which the observed "true polar wander" refers, are essentially the same. If hotspots move in a convecting mantle, this is not necessarily the case, and we have previously computed how the observed "true polar wander" curve changes when it is converted to a mean mantle reference frame, taking computed hotspot motions into account [*Steinberger and O'Connell*, 2000]. Since the difference turned out to be small, it will be disregarded for the purpose of this paper.

1.2. Changes of the Earth's Rotation Axis - Dynamic Modelling

The subject of long-term changes in the Earth's rotation axis and its relation to mass redistributions inside the Earth has a rather long history. The idea that the rotation axis might significantly change relative to some reference frame tied to the solid Earth, and that, for example, poles might move to where the equator used to be, and vice versa, was proposed much earlier than plate tectonics.

Darwin [1876] made the first quantitative attempt to deal with changes of the Earth's axis of rotation due to geological changes. Darwin tried to solve the problem of how the rotation axis changes if there is an uplift of material at some area at the Earth's surface. He arrived at the result that a change in the rotation axis is possible. However his work was marred by several errors. The first one is an algebraic error discovered by *Lambert* [1931]. The correction is given by *Jeffreys* [1952] on page 343. With this correction, the conclusion is reversed, and the rotation axis should not move a significant amount. In addition, Darwin made another error in assuming that the axis of the geoid (as defined by *Gold* [1955]) moves towards the rotation axis at a rate proportional to the separation of the axis of figure (following *Gold* [1955] defined as the principal axis of the inertia tensor with the largest moment of inertia) and the rotation axis. This error is pointed out by *Munk* [1956]. His paper reviews Darwin's paper, its errors, and the discussions it sparked during the 55 years until the first error was detected.

The first qualitatively correct treatment is given by *Gold* [1955]. He describes how an excess mass that is added to the Earth leads to a slow deformation of the Earth and a change of the rotation axis, causing the excess mass to move slowly toward the equator (without being displaced relative to the solid Earth). This process is described in Figure 1, where four excess masses are added, such that the center of mass does not change, and only one non-diagonal inertia tensor element changes due to the excess masses.

Gold's paper inspired *Burgers* [1955] to treat the problem quantitatively. Burgers considers a homogeneous viscoelastic sphere, the moments of inertia of which are changed by a small amount. He arrives at a solution, which consists of small oscillations ("wobble") of the rotation axis and a long-term mean motion. The subject is reviewed by *Inglis* [1957].

Munk and MacDonald [1960] discuss how an approximate solution for a layered sphere may be obtained using the concept of Love numbers assuming a Maxwell viscoelastic rheology. More recently, calculations for a layered viscosity structure have been done. *Sabadini et al.* [1982] treat the changes of the Earth's rotation in response to growing and melting of large ice sheets. They look at an Earth model composed of an elastic lithosphere, a viscoelastic mantle and an inviscid core, i.e. a three-layer-model. They treat the equations by doing a Laplace transform and calculating eigenmodes of the relaxation. *Wu and Peltier* [1984] perform a similar kind of analysis, but they arrive at a different result. They claim that *Sabadini et al.* [1982] did an invalid

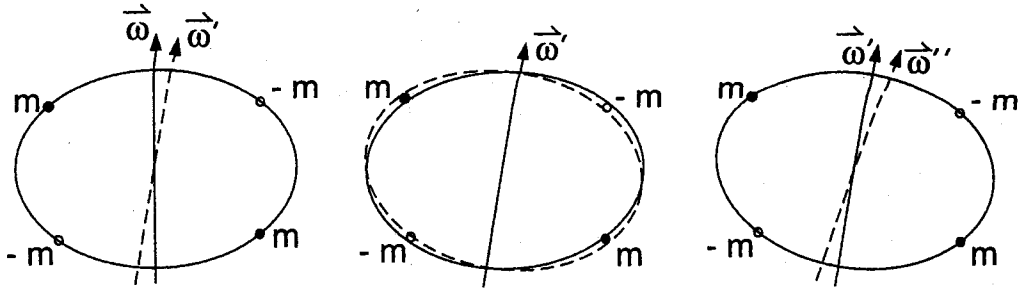

Figure 1. Interplay between deformation and change of the rotation axis of the Earth. First picture: Non-hydrostatic excess masses cause the rotation axis of the Earth to change (from the solid to the dashed line). Second picture: The change in rotation axis causes the Earth to deform (from solid to dashed outline). Third picture: This change in shape causes the rotation axis to move again. The process would cease once it has shifted the excess masses to the equator, but this is only approached asymptotically.

approximation. *Sabadini et al.* [1984] provide a more general treatment and show that the two formulations are equivalent to some extent. They also point out that a solution requires in addition to the eigenmodes of viscoelastic relaxation another set of eigenmodes arising from the coupling of viscoelastic relaxation and rotational dynamics. *Mitrovica and Milne* [1998] give a detailed comparison of the two approaches by *Sabadini et al.* [1982] and *Wu and Peltier* [1984] and show, using a generalized theory, that the two formalisms yield essentially equivalent predictions.

Sabadini and Yuen [1989] state that the rate of change in the rotation axis depends on the viscosity structure and on the chemical structure (i.e. non-adiabatic density variations). They emphasize that the change of the rotation axis over long times can put constraints on both chemical stratification and viscosity distribution in the mantle and that there are trade-offs between the style of mantle chemical stratification and the magnitude of lower mantle viscosity. *Ricard et al.* [1992] investigate how the nature of the 670-km-discontinuity affects the rate of change of the rotation axis. In their calculations, a phase change yields a large rate of change, whereas the rate is drastically reduced for chemically stratified models. They use the linearized Liouville equations valid for small displacements and express viscoelastic deformation in terms of eigenmodes. *Spada et al.* [1992] compute changes of rotation due to subduction using an asymptotic expansion for large time of the nonlinear Liouville equations for an Earth model consisting of an elastic lithosphere, a Maxwell viscoelastic mantle and an isostatic core. They show that a viscosity increase with depth is required to achieve realistic rates of polar wander. Using a viscous quasi-fluid approximation, *Ricard et al.* [1993] further discuss the change of the rotation axis induced by a downgoing cold slab, depending on the viscosity structure.

More recently, *Fang and Hager* [1995] have shown that for a realistic Earth model with continuously varying density, viscosity and elastic parameters, viscoelastic relaxation cannot be solely expressed in terms of discrete eigenmodes, and the error made by only considering discrete modes depends on the exact viscosity structure. This problem arises because of the so-called "Maxwell singularities". For this reason, *Hanyk et al.* [1995] proposed a "time-domain approach for the transient responses in stratified viscoelastic Earth models". On the other hand, Boschi et al. [1999] showed how the problem of Maxwell singularities can be avoided, and that hence the eigenmode approach is still valid.

Here we develop an independent and entirely self-contained algorithm which allows us to use both time-domain and eigenmode approach to calculate changes of the Earth's rotation axis for a rather general viscoelastic Earth model in an efficient manner. The algorithm is developed and results are presented in section 2. We will first show that a quasi-static approximation, i.e. disregarding differences between the axis of figure and the rotation axis, which give rise to the "Chandler wobble" [*Ricard et al.* 1993] and direct integration give virtually identical results. We thus verify that the derivation and numerical implementation of the equations for quasi-static integration has been done correctly. We will compare the results of the time domain and eigenmode approach and show that for the cases considered here differences are much smaller than other uncertainties in the model. We will also discuss in which cases a "steady-state approach", which allows an even more effective computation, is suitable. In the end, we will calculate changes in the rotation axis caused by advection of realistic density anomalies inferred from seismic tomography in a realistic flow field [*Hager and O'Connell*, 1979, 1981]. Our approach is similar to the one pursued by *Richards et al.* [1997], except that they use models of

subduction history instead of mantle flow models based on seismic tomography in order to compute changes of the moment of inertia tensor. Thus their approach only includes the effect of downgoing slabs, whereas our approach implicitly captures all sources of the changing density distribution. The difference is probably significant, because mantle flow is likely not only driven by downgoing slabs but also includes active upwellings [*Gurnis et al.*, 2000].

Along a different line of thought, *Goldreich and Toomre* [1969] discuss some statistical aspects of the change of the rotation axis in time. They make the assumption that the equatorial bulge does not hinder a change in the rotation axis, and thus the rotation axis always follows the axis of maximum non-hydrostatic moment of inertia. They then simulate a randomly evolving, almost spherical body. They find, that the rotation axis changes rapidly when two of the principal non-hydrostatic moments of inertia become almost equal, because then the principal axes of the non-hydrostatic inertia tensor move most rapidly. The procedures outlined in this work allow us to calculate how rapid this change may be, and obtain the maximum speed of change in the case when the two larger principal moments of inertia become equal or almost equal ("inertial interchange"). These results were already shown by *Steinberger and O'Connell* [1997] where it was also shown that under normal circumstances the rotation axis will indeed follow the axis of maximum non-hydrostatic moment of inertia very closely, thus justifying the assumption made by *Goldreich and Toomre* [1969].

1.3. Changes of the Earth's Rotation Axis - Observational Aspects

Early work suggested that in the mean lithospheric frame there occurs no significant change of the rotation axis [*McElhinny*, 1973; *Jurdy and van der Voo*, 1974], whereas there is a change of the hotspot frame with respect to the rotation axis [*Duncan et al.*, 1972]. This led to the "mantle roll" hypothesis [*Hargraves and Duncan*, 1973]: The rotation axis is fixed relative to the mean lithosphere, whereas the lower mantle "rolls" relative to both of them. *Jurdy* [1981] points out that the previous works cannot be compared directly, because they use different datasets. By using the same dataset in both cases she rules out that the different results are due to different data. She finds no significant motion of the rotation pole relative to the mean lithosphere, but a large motion of 10 - 12 degrees relative to the hotspots since early Tertiary, thus confirming the mantle roll hypothesis.

More recently however this hypothesis has been questioned. *Gordon and Jurdy* [1986] showed that both reference frames are more similar than previously thought and suggest that both reference frames and the paleomagnetic axis might be in relative motion, however with the paleomagnetic-hotspot motion probably larger than the relative motion of mean lithospheric and hotspot reference frame. *Gordon and Livermore* [1987] extended the analysis into the late Cretaceous and reported that in both the mean lithospheric and in the hotspot reference frame the rotation axis has shifted by $10° - 20°$ in the same direction during the last 100 m.y.

Published true polar wander paths usually show the motion of the pole in the African hotspot reference frame [*Andrews*, 1985, *Besse and Courtillot*, 1991, *Prevot et al.*, 2000]. Despite some differences, recent results agree on the following general features:

- Fast polar motion of a few degrees during the past few Myr, roughly towards Greenland. This is most likely due to glacial effects.
- Slow motion (if any) of a few degrees at most (i.e., less than the few degrees uncertainty of a paleomagnetic determination) in a similar direction, during the Tertiary.

In this work, we will compare the calculated motion of the rotation axis with the most recent results of *Besse and Courtillot* [2000, pers. comm.] and *Prevot et al.* [2000]. Both these results also agree on faster motion prior to about 60 to 90 Ma in a roughly opposite direction, but *Tarduno and Smirnov* [2001] argue that the rotation axis has moved by no more than $\sim 5°$ over the last 130 million yr and that the apparent polar shift in reality represents hotspot motion. The required relatively fast hotspot motion does not agree with modelling results [e.g. *Steinberger*, 2000], however models of mantle flow, and hence hotspot motion, become rather unreliable prior to the Tertiary: This is also evidenced by the predictions of polar motion due to mantle flow presented in section 3.

2. CHANGE OF THE EARTH'S ROTATION AXIS DUE IMPOSED CHANGES OF THE INERTIA TENSOR

2.1. Overview

In this section we will develop a quantitative treatment of the process that was first qualitatively explained by *Gold* [1955]). This requires a coupled solution of two problems: How a change of the rotation axis causes a deformation of the Earth, and how a deformation of the Earth causes a change of the rotation axis. The first part is a continuum mechanics problem, the second part is a problem of rotational dynamics.

We will first develop a formalism to solve the first problem separately: For a given change of the rotation vector, what is the deformation that results for an Earth model consisting of a mantle with Maxwell viscoelastic rheology overlying a hydrostatic core? The formulation will first be given in the Laplace transform domain, where the governing equations can be written in the form of a linear system of ordinary differential equations. This allows us to compute eigenfunctions of viscoelastic decay. However we do not restrict ourselves to the eigenfunction approach. We will therefore transform the equations back into time domain and show how any viscoelastic deformation consists of an immediate elastic deformation corresponding to the change in the rotation axis and a slow viscoelastic deformation corresponding to the deviation of the actual shape from equilibrium shape. We will show how to compute the equilibrium shape, the immediate elastic deformation following a change in rotation and the slow viscoelastic deformation in the time domain. Our formulation is similar to the equations for viscous flow given by *Hager and O'Connell* [1979, 1981]. A far more detailed derivation of this formalism is given by *Steinberger* [1996], whereas here only the principal steps are recapitulated.

This formalism will then be combined with the equations of motion of a rotating body in a rotating frame of reference (Euler equations, often also referred to as Liouville equations in the case of a deformable body). A method to integrate the Euler equations efficiently will be presented. This method will be used to calculate changes in the Earth's rotation axis for various cases. For simplicity a distribution of excess masses as in Figure 1 will be used.

2.2. *Deformation of the Earth due to a Change in Rotation – Formulation for Viscoelastic Relaxation in the Mantle in the Laplace Transform Domain*

Time derivatives in the constitutive relationship of a Maxwell-body can be eliminated by performing a Laplace transform. By doing so, each time derivative operator $\frac{\partial}{\partial t}$ is replaced by the Laplace transform variable s.

Changes of the rotation vector only excite displacements $\delta\mathbf{u}$, stress anomalies $\delta\mathbf{T}$, potential anomalies $\delta\varphi$ and density anomalies $\delta\rho$ of spherical harmonic degree two and zero. Since we only deal with changes of the rotation axis without changing the rotation rate, we can neglect degree zero terms. Therefore the spherical harmonic expansions simplify to

$$
\begin{aligned}
\delta u_r &= \sum_{m=-2}^{2} u_{1,2m} Y_{2m} \\
\delta u_\theta &= \sum_{m=-2}^{2} u_{2,2m} \frac{\partial Y_{2m}}{\partial \theta} \\
\delta u_\phi &= \sum_{m=-2}^{2} u_{2,2m} \frac{1}{\sin\theta} \frac{\partial Y_{2m}}{\partial \phi} \\
\delta T_{rr} &= \frac{\alpha_0}{r} \sum_{m=-2}^{2} u_{3,2m} Y_{2m} \\
\delta T_{r\theta} &= \frac{\alpha_0}{r} \sum_{m=-2}^{2} u_{4,2m} \frac{\partial Y_{2m}}{\partial \theta} \\
\delta T_{r\phi} &= \frac{\alpha_0}{r} \sum_{m=-2}^{2} u_{4,2m} \frac{1}{\sin\theta} \frac{\partial Y_{2m}}{\partial \phi} \\
\delta\varphi &= \frac{\alpha_0}{\rho_{00} r} \sum_{m=-2}^{2} u_{5,2m} Y_{2m} \\
\frac{\partial \delta\varphi}{\partial r} &= \frac{\alpha_0}{\rho_{00} r^2} \sum_{m=-2}^{2} u_{6,2m} Y_{2m}
\end{aligned}
\tag{1}
$$

where ρ_{00} and α_0 are numerical constants, and Y_{2m} are (unnormalized) spherical harmonics.

After omitting indices $2m$ and combining $u_1 \ldots u_6$ to a vector $\mathbf{u}$ (which is not identical to $\delta\mathbf{u}$), the governing equations are transformed into a matrix equation for spherical harmonic degree two:

$$
\frac{d\mathbf{u}}{dr} = \frac{1}{r}\mathbf{M}\cdot\mathbf{u} + \mathbf{b}_1. \tag{2}
$$

Without loss of generality it is assumed that the rotation vector ω is aligned with the z-axis. Then the vector $\mathbf{b}_1$, which depends on ω^2, only appears for order $m = 0$. Explicit expressions for $\mathbf{b}_1$ and the matrix $\mathbf{M}$ are given by *Steinberger* [1996].

2.3. *Equations for Viscoelastic Relaxation in the Time Domain*

The equation (2) can be symbolically restored to the time domain by replacing s by $\frac{\partial}{\partial t}$ after algebraic rearrangement. We can thus obtain

$$
\begin{aligned}
&\frac{\partial}{\partial t}\left(\frac{d\mathbf{u}}{dr} - \frac{1}{r}\mathbf{M}_2\mathbf{u}\right) = \\
&\frac{\mu}{\eta}\left(-\mathbf{M}_3\frac{d\mathbf{u}}{dr} + \frac{1}{r}\mathbf{M}_4\mathbf{u} + \mathbf{b}_3\right) + \frac{\partial}{\partial t}\mathbf{b}_1
\end{aligned}
\tag{3}
$$

$\mathbf{M}_2$ is analogous to $\mathbf{M}$ in eqn. (2) in the purely elastic case. The vector $\mathbf{b}_3$ depends on ω^2; and only appears for order $m = 0$; $\frac{\partial}{\partial t}\mathbf{b}_1$ depends on $\omega \cdot \frac{d\omega}{dt}$, and since we neglect changes in the magnitude of ω, it only appears for orders $m = 1$ and $m = -1$. Explicit expressions

for $\mathbf{b}_3$ and $\frac{\partial}{\partial t}\mathbf{b}_1$ and the matrices $\mathbf{M}_2$, $\mathbf{M}_3$ and $\mathbf{M}_4$ are given by *Steinberger* [1996].

We solve equations (3) by splitting $\mathbf{u}$ into an equilibrium value $\mathbf{u}_{eq}$ and a departure from equilibrium $\mathbf{u}_{ne}$. Equations for the hydrostatic equilibrium shape [*Clairaut*, 1743] can be given in the form of a 2×2 matrix equation compatible with eqn. (2):

$$\begin{aligned} \frac{d}{dr}\begin{pmatrix} u_5 \\ u_6 \end{pmatrix} &= \frac{1}{r}\mathbf{M}_{eq}\begin{pmatrix} u_5 \\ u_6 \end{pmatrix} + \mathbf{b}_2 \qquad (4) \\ u_3 &= \rho_0/\rho_{00} \cdot u_5 + b_{14} \\ u_4 &= 0, \end{aligned}$$

where ρ_0 is the density of the reference Earth model. $\mathbf{b}_2$ and b_{14}, which depend on ω^2, only appear for order $m = 0$, however when computing the time derivative of eqn. (4), $\frac{\partial}{\partial t}\mathbf{b}_2$ and $\frac{\partial}{\partial t}b_{14}$ only appear for orders $m = 1$ and $m = -1$. Explicit expressions for $\mathbf{b}_2$, $\frac{\partial}{\partial t}\mathbf{b}_2$, b_{14}, $\frac{\partial b_{14}}{\partial t}$, and $\mathbf{M}_{eq}$, are given by *Steinberger* [1996]. These equations only depend on density structure, not on compressibility, rigidity or viscosity. In the case of a non-adiabatic density structure, expressions for u_1 and u_2 in terms of u_5, u_6 and ω^2, can be found for the mantle [*Steinberger*, 1996]. For an adiabatic density structure, equilibrium values of u_1 and u_2 are not uniquely defined, but the same expressions may still be used. The expression for u_1 then means the elevation of the equipotential surface from its spherical reference shape.

Hence (3) can be brought into the form

$$\frac{\partial}{\partial t}\left(\frac{d\mathbf{u}}{dr} - \frac{1}{r}\mathbf{M}_2\mathbf{u}\right) = \frac{\partial}{\partial t}\mathbf{b}_1 + \frac{\mu}{\eta}\left(-\mathbf{M}_3\frac{d\mathbf{u}_{ne}}{dr} + \frac{1}{r}\mathbf{M}_4\mathbf{u}_{ne}\right) \qquad (5)$$

(Note that $\mathbf{u}$ still appears on the left-hand-side, whereas $\mathbf{u}_{ne}$ appears on the right-hand-side). The change in shape therefore consists of two parts: An immediate elastic change and a slow viscoelastic change (corresponding to the second and third term on the r.h.s.)

In the mantle and crust we therefore solve eqn. (5) by expressing the change in $\mathbf{u}$ as sums of two terms: $\frac{\partial \mathbf{u}}{\partial t} = \dot{\mathbf{u}}_a + \dot{\mathbf{u}}_b$, with

$$\frac{d\dot{\mathbf{u}}_a}{dr} - \frac{\mathbf{M}_2\dot{\mathbf{u}}_a}{r} = \frac{\partial \mathbf{b}_1}{\partial t} \quad \text{and} \qquad (6)$$

$$\frac{d\dot{\mathbf{u}}_b}{dr} - \frac{\mathbf{M}_2\dot{\mathbf{u}}_b}{r} = \frac{\mu}{\eta}\left(-\mathbf{M}_3\frac{d\mathbf{u}_{ne}}{dr} + \frac{\mathbf{M}_4\mathbf{u}_{ne}}{r}\right) \qquad (7)$$

Similarly we solve eqn. (4) in the core by splitting the change in $\mathbf{u}_2$ and u_3: $\frac{\partial \mathbf{u}_2}{\partial t} = \dot{\mathbf{u}}_{2,a} + \dot{\mathbf{u}}_{2,b}$ and $\frac{\partial u_3}{\partial t} = \dot{u}_{3,a} + \dot{u}_{3,b}$, with

$$\frac{d\dot{\mathbf{u}}_{2,a}}{dr} - \frac{1}{r}\mathbf{M}_{eq}\dot{\mathbf{u}}_{2,a} = \frac{\partial \mathbf{b}_2}{\partial t}, \quad \dot{u}_{3,a} = \frac{\rho_0}{\rho_{00}}\dot{u}_{5,a} + \frac{\partial b_{14}}{\partial t} \qquad (8)$$

$$\frac{d\dot{\mathbf{u}}_{2,b}}{dr} - \frac{1}{r}\mathbf{M}_{eq}\dot{\mathbf{u}}_{2,b} = 0, \quad \dot{u}_{3,b} = \frac{\rho_0}{\rho_{00}}\dot{u}_{5,b}. \qquad (9)$$

Eqns. (6) and (8) describe the immediate elastic deformation, (7) and (9) the slow viscoelastic deformation.

The viscosity appears in none of the matrices. Therefore, the speed of viscoelastic relaxation is inversely proportional to viscosity: If viscosity is increased by a factor n everywhere, the speed of viscoelastic relaxation decreases by a factor $1/n$ everywhere. With boundary conditions prescribed at the surface and internal interfaces, as well as a regularity condition at the center of the Earth, we are now able to separately solve for equilibrium shape, immediate elastic, and slow viscoelastic deformation. A detailed treatment of these boundary conditions was given by [*Steinberger*, 1996] and is not repeated here.

For the equilibrium shape, we may find two independent solutions which satisfy the regularity condition at the center, and can construct a general solution with one free parameter by linear superposition. The free parameter is determined by matching the gravity boundary condition (corresponding to "all sources of gravity within") at the surface.

For the elastic deformation we can similarly find a general solution with one free parameter in the core. In the mantle, we can find a general solution with four free parameters, which satisfies the boundary conditions $\dot{u}_{3,a} = \rho_0/\rho_{00}\dot{u}_{5,a} + \frac{\partial}{\partial t}b_{14}$ and $\dot{u}_{4,a} = 0$ below the core-mantle boundary. The free parameters (five in total) are determined by matching the three surface boundary conditions (no normal or tangential stress; all sources of gravity within) and enforcing continuity of potential and gravity across the core-mantle boundary. There is no continuity requirement for displacement, since it is undetermined in the core. The theory of elastic deformation has been established long ago, in the context of calculating the free oscillations of the Earth. *Alterman et al.* [1959] use a formalism similar to ours.

For a known right-hand-side vector the solution for $\dot{u}_b$ can be obtained in an analogous way. However in this case, the right-hand side does not only depend on the current change of rotation, but on the whole previous history of rotation. Starting from given initial values of $\mathbf{u}$ in the mantle and $\mathbf{u}_2$ in the core, values at any time can be calculated with a numerical time integration. At each time integration step, $\dot{u}_b$ and $\dot{u}_{2,b}$ are calculated with a radial integration analogous to the elastic case. These time derivatives are then used to calculate changes in $\mathbf{u}$ and $\mathbf{u}_2$. $\mathbf{u}$ and $\mathbf{u}_2$ and their time derivatives are expressed in terms of radial basis functions, and the time integration is performed on the expansion coefficients. For basis functions, we ei-

ther use eigenfunctions of viscoelastic decay, which are described in the next section, or Chebychev polynomials. If eigenfunctions are used, the equations decouple for each coefficient. Results on how the inertia tensor would change over time due to slow viscoelastic deformation following an instantaneous change in rotation after initial hydrostatic equilibrium will be presented in section 2.5 together with results on changes in the rotation axis obtained by integrating the Euler equations.

2.4. *Eigenfunctions of Viscoelastic Decay*

If a solution can be expressed in terms of exponentially decaying eigenfunctions $\mathbf{u}(t) = \mathbf{u}_0 e^{-st}$, we can calculate these by solving eqn. (2) without the inhomogeneous term:

$$\frac{d\mathbf{u}}{dr} = \frac{1}{r}\mathbf{M}\cdot\mathbf{u} \tag{10}$$

Solutions to this equation only exist for certain decay rates. For example, in the case of a viscous, incompressible mantle with layers of constant density we can, at any time, expand $\mathbf{u}_{ne}$ in terms of eigenfunctions of viscoelastic (in this case: viscous) decay. In this case, the displacements of the boundaries from the equilibrium value drive the flow towards equilibrium. In the case of n layers, there are n eigenfunctions, and we can express the boundary displacements in terms of eigenfunctions exactly. For example, in the case of a mantle of constant density underlain by a core of higher constant density, there are two eigenfunctions. These modes have been termed M0 and C0 in the literature [*Peltier*, 1976]. The corresponding decay times (inverse of decay constant s) depend on viscosity structure. Figure 2 shows the radial displacement u_1 as a function of radius for the eigenmodes of several viscous Earth models. Whereas a decrease in upper mantle viscosity leads to only a slight decrease in decay times, a viscosity increase in a substantial part of the lower mantle leads to a substantial increase in decay times. Figure 3 shows sketches of the displacement field for the two modes M0 and C0.

Each chemical boundary with a density jump within the mantle introduces an additional mode. These modes are characterized by long decay times and called M1, M2, ... [*Peltier*, 1976]. An example is shown in the bottom right panel of Figure 2, where at depth 670 km a jump in density equal to the density jump in PREM is introduced. One question that we will address later is whether the presence of the M1 mode etc. with its long decay time will significantly affect the maximum speed at which the Earth's rotation axis may change.

In the case of a compressible mantle with Maxwell rheology, further modes and series of modes arise. These modes are apparently first reported by *Han and Wahr* [1995], where they are termed "compressible modes". They were also found by *Vermeersen et al.* [1996], and we have previously given examples of viscoelastic mode spectra as well [*Steinberger*, 1996]. These are not included here, because we show that despite all the complication, in many cases for an approximately adiabatic Earth model (such as PREM) consideration of only the two fundamental modes M0 and C0 leads to a good approximation in computing true polar wander.

2.5. *Integrating the Euler Equations for a Rotating, Self-Gravitating Viscoelastic Body*

In the absence of external torques, the equation governing changes of the rotation vector can be written in the form

$$\frac{dJ_{il}}{dt}\cdot\omega_l + J_{il}\cdot\frac{d\omega_l}{dt} = -\varepsilon_{ijk}\omega_j\cdot J_{km}(t)\cdot\omega_m(t). \tag{11}$$

ω_i are the components of the angular velocity vector, which describes the rotation of the frame of reference in "absolute space" (note that for rotation the concept of "absolute space" makes sense, whereas it makes no sense for translatory motion).

The inertia tensor can be expressed in terms of the five degree two components of $u_5(r_E)$ as defined in equation (1) [*Steinberger*, 1996]:

$$\mathbf{J} = J_{ss}\mathbf{I} + \frac{r_E^2\alpha_0}{\rho_{00}G}\cdot\begin{pmatrix} T_{11} & T_{12} & T_{13} \\ T_{21} & T_{22} & T_{23} \\ T_{31} & T_{32} & T_{33}\end{pmatrix} \tag{12}$$

J_{ss} is the moment of inertia for the spherically symmetric reference shape, G is the gravity constant,

$$\begin{aligned}
T_{11} &= -\tfrac{1}{3}u_{20,5}(r_E) + 2u_{22,5}(r_E)\\
T_{12} &= 2u_{2-2,5}(r_E)\\
T_{13} &= u_{21,5}(r_E)\\
T_{21} &= 2u_{2-2,5}(r_E)\\
T_{22} &= -\tfrac{1}{3}u_{20,5}(r_E) - 2u_{22,5}(r_E)\\
T_{23} &= u_{2-1,5}(r_E)\\
T_{31} &= u_{21,5}(r_E)\\
T_{32} &= u_{2-1,5}(r_E)\\
T_{33} &= \tfrac{2}{3}u_{20,5}(r_E)
\end{aligned}$$

and the first index group of u is referring to the spherical harmonic (20, 21, 2-1, 22 or 2-2) and the second index to the component 5.

J can be split up into a hydrostatic equilibrium part and a non-hydrostatic part. We also split the *total* non-hydrostatic part up into (1) a contribution *imposed* by mantle convection – this would be the only part if the Earth wasn't rotating, and (2) a contribution caused by the change of the rotation axis and the immedi-

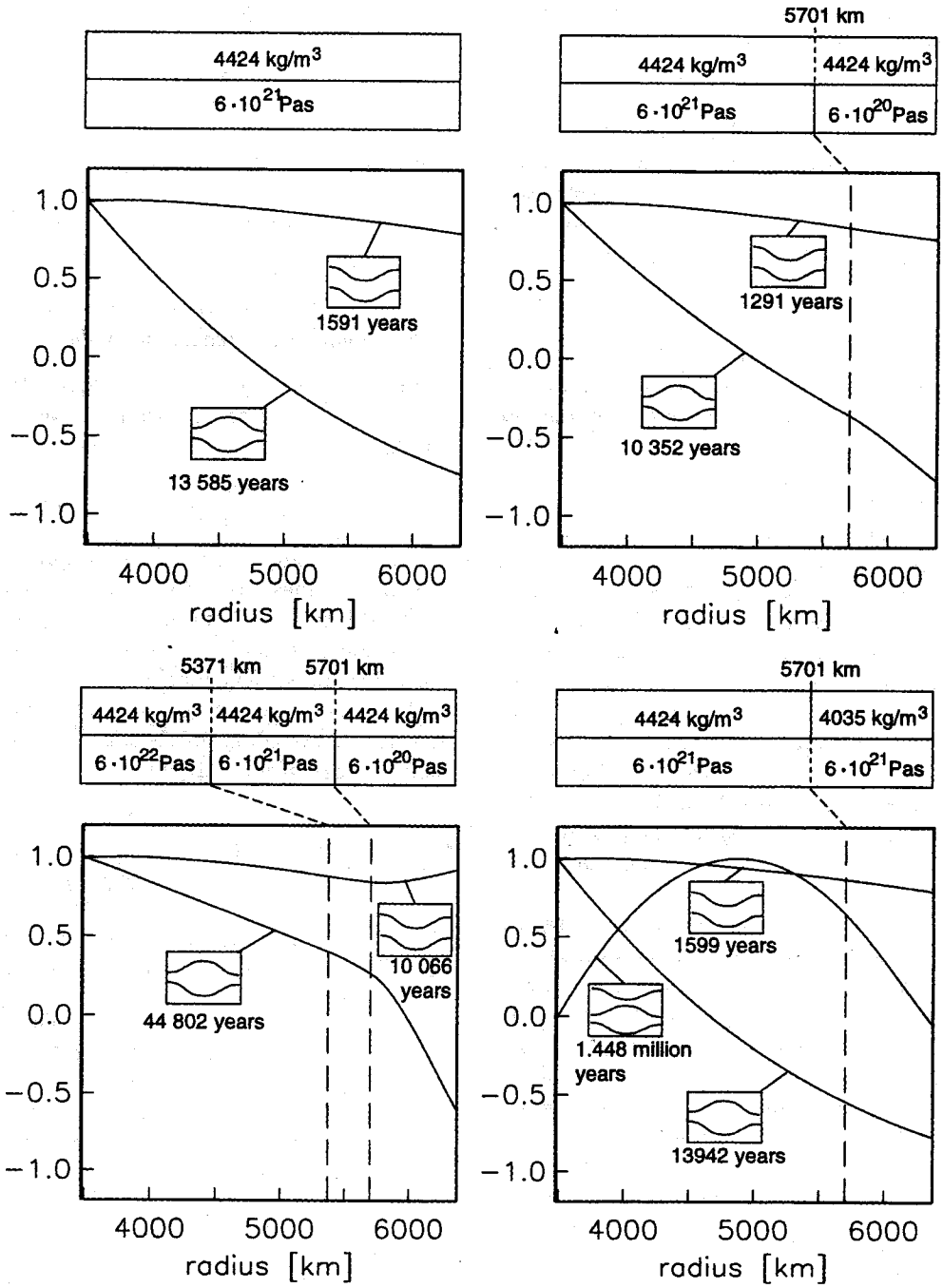

Figure 2. Radial displacement of eigenmodes as function of radius for several Earth models. All models consist of a core (radius 3480 km) of density 10 989 kg m^{-3} in hydrostatic equilibrium and a viscous incompressible mantle. Mantle density and viscosity structure is indicated for each model. All functions are normalized to a maximum value of 1. Corresponding displacement fields are indicated by the sketches in the small rectangles; corresponding decay times are shown below the rectangles.

ate elastic and delayed viscoelastic adjustment to the new equilibrium shape. In this section we will calculate changes of the rotation axis caused by initially *imposed* non-hydrostatic inertia tensor elements, which may be due to excess masses such as in Figure 1 or sinking "slablets" such as discussed by *Ricard et al.* [1993]. The axis of maximum hydrostatic moment of inertia is by definition parallel to the rotation axis, and one

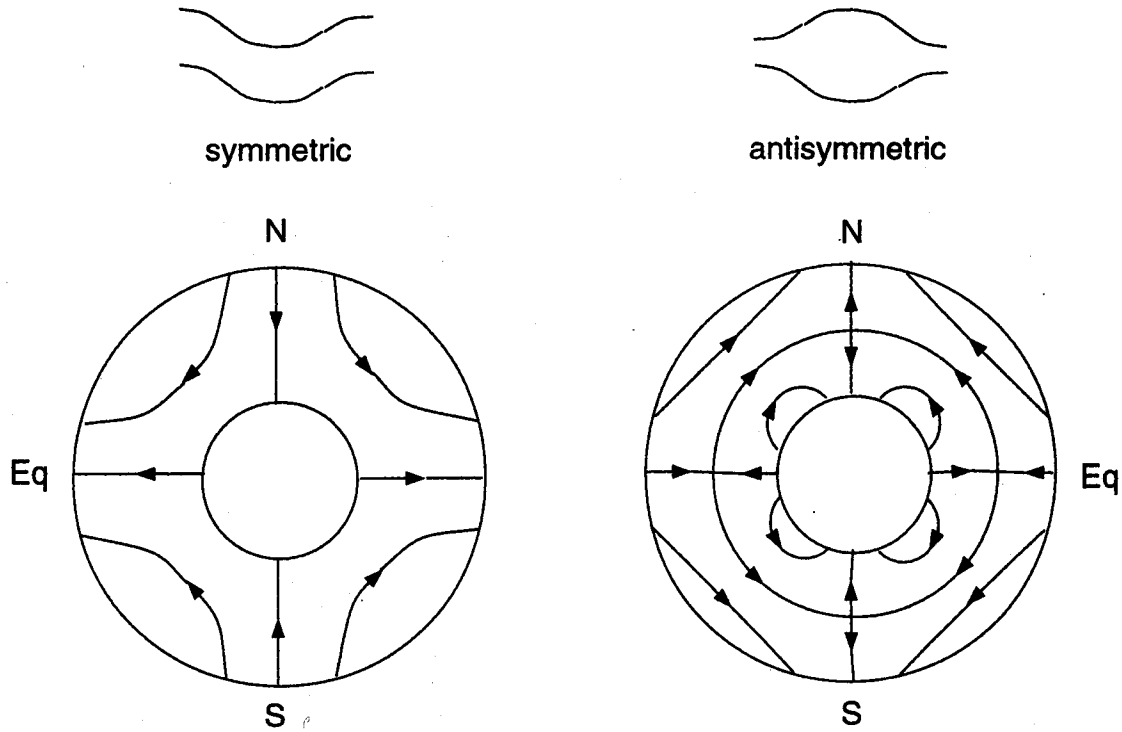

Figure 3. Sketch of displacement field (degree two, order zero) for the viscous modes M0 (left) and C0 (right) (polar cross section with core radius not to scale).

of the principal axes of the *total* non-hydrostatic inertia tensor always follows the rotation axis closely. This latter statement is actually not self-evident. *Spada et al.* [1996a, b] show that for Venus, which is rotating much more slowly than Earth, significant separations of more than 1° may occur, but for the Earth, a separation of only about 0.001″ can be expected to be caused by mass redistributions due to mantle flow, whereas the observed separation related to the Chandler wobble is about 0.3″. Usually, it will be the principal axis with the maximum total non-hydrostatic moment of inertia (axis of figure), which is approximately aligned with the rotation axis, but not always, as was pointed out by *Ricard et al.* [1993]: Because of delays in the adjustment of the equatorial bulge, it may be one of the other principal axes for some period of time. However this approximate alignment does not imply an alignment of the rotation axis with the axis of maximum *imposed* non-hydrostatic moment of inertia; due to the same reason of delayed adjustment of the equatorial bulge, a misalignment may result.

We will now present several methods of integrating the Euler equations:

- Direct numerical integration, using no further approximations
- "Quasi-static" numerical integration, assuming the rotation axis is always exactly parallel to the axis of figure.
- Analytical "steady-state" solution, additionally assuming that the "build-up" of non-equilibrium shape is always exactly compensated by viscoelastic decay.

For direct integration the adopted time steps have to be quite small, since the rotation vector changes with the period of the Chandler wobble ($\approx$ 1 year). We will therefore compare direct and "quasi-static" integration for a simple viscous Earth model and show that there is very good agreement. This justifies using the quasi-static integration. With this method, which is $O(10^3)$ times faster, integration also becomes feasible for more complicated viscoelastic Earth models, which require many more variables to be time-integrated. We will compare several viscous and viscoelastic cases. As it turns out, the speed with which the rotation axis may change mostly depends on the viscosity structure. We will also use an example to show that except for an initial period of adjustment the "steady-state" assumption is valid. In the last part we will therefore use the analytical method to compare several viscous Earth models.

2.5.1. Direct integration. The change of the inertia tensor in eqn. (11) consists of a part due to elastic deformation $\left.\frac{d\mathbf{J}}{dt}\right|_{el}$ and a part due to viscoelastic deformation $\left.\frac{d\mathbf{J}}{dt}\right|_{ve}$. The part due to elastic deformation depends only on the change in the rotation vector. We can therefore write

$$\frac{dJ_{il}}{dt} = \frac{\partial J_{il}}{\partial \omega_n}\frac{d\omega_n}{dt} + \left.\frac{dJ_{il}}{dt}\right|_{ve} \tag{13}$$

$\frac{\partial J_{il}}{\partial \omega_n}$ is a third-order tensor. If we call $u_5(r_E) = u_{el}$ in the case corresponding to a change from no rotation to a rotation around the z-axis at the present rate (to obtain a solution for this case, in eqns. (6) and (8) $\dot{u}_a$, $\dot{u}_{2,a}$, $\dot{u}_{3,a}$, $\frac{\partial}{\partial t}\mathbf{b}_1$, $\frac{\partial}{\partial t}\mathbf{b}_2$ and $\frac{\partial}{\partial t}b_{14}$ have been replaced by $\mathbf{u}$, $\mathbf{u}_2$, u_3, $\mathbf{b}_1$, $\mathbf{b}_2$ and b_{14} respectively) then in a coordinate system with the z-axis aligned with the rotation axis, it is

$$\frac{\partial J_{il}}{\partial \omega_n} = u_{el}\cdot\frac{r_E^2\alpha_0}{\rho_{00}G}\cdot K_{iln}, \tag{14}$$

with

$$K_{iln} = \begin{cases} 1 & \text{for } iln = 131, 311, 232, 322 \\ -2/3 & \text{for } iln = 113, 223 \\ 4/3 & \text{for } iln = 333 \\ 0 & \text{otherwise} \end{cases}$$

However we will solve the Euler equations in a coordinate system that is fixed to the body and therefore have to transform them accordingly.

If we insert (13) into (11) we obtain

$$\left(\frac{\partial J_{il}}{\partial \omega_n}\omega_l + J_{in}\right)\frac{d\omega_n}{dt} = -\varepsilon_{ijk}\omega_j\cdot J_{km}\cdot\omega_m - \left.\frac{dJ_{il}}{dt}\right|_{ve}\omega_l \tag{15}$$

If we now define M_{pi}^{-1} such that $M_{pi}^{-1}\cdot\left(\frac{\partial J_{il}}{\partial \omega_n}\omega_l + J_{in}\right) = \delta_{pn}$ (i.e. M_{pi} can be calculated by matrix inversion) we have

$$\frac{d\omega_n}{dt} = M_{ni}^{-1}\cdot\left(-\varepsilon_{ijk}\omega_j\cdot J_{km}\cdot\omega_m - \left.\frac{dJ_{il}}{dt}\right|_{ve}\omega_l\right) \tag{16}$$

Eqn. (16) enables us to find the change of the rotation vector, given the rotation vector itself, the inertia tensor and the viscoelastic part of its time change. But eqns. (5) and (12) allow us to calculate the inertia tensor and the viscoelastic part of its time change, given the rotation vector and the present values of the vector $\mathbf{u}$ for all five degree-two spherical harmonics. With this, we can state the Euler equations as a system of first-order ordinary differential equations for the three components of the rotation vector and some parameters which specify the radial functions. In the case of an incompressible viscous medium with n layers of constant density, for each of the five spherical harmonics, n parameters are necessary for specification. For example, the departure of boundary displacements from equilibrium, or the coefficients of the expansion of $\mathbf{u}_{ne}$ in terms of the n eigenfunctions of viscoelastic decay may be chosen.

Figure 4 shows results of a direct integration. As can be seen, even if the rotation axis and axis of figure initially agree, the calculated curve of the pole is not a straight line. It is rather a cycloid curve (a curve describing the motion of a point on the perimeter of a rolling wheel). Comparison of the elastic and viscoelastic cases shows

- an increase of the Chandler wobble period from about 290 days to about 450 days (a well-known effect)
- an increase of the Chandler wobble amplitude by about the same factor
- a slight decrease of the secular drift rate of the pole.

The first two effects are mainly due to immediate elastic deformation, apart from the different density structure. The third effect is only initially present and is reversed for longer time integration, as we will see. Direct comparison for the same density structure is not possible, since an incompressible mantle of constant density corresponds to an adiabatic viscoelastic mantle. The PREM lower mantle, which is used here in the viscoelastic case is approximately adiabatic.

2.5.2. Quasi-static integration. Following *Ricard et al.* [1993] we now assume that the rotation axis is aligned with one of the principal axes of the inertia tensor, which shall be the z-axis (therefore $\omega_1 = \omega_2 = 0$; $\omega_3 =: \omega_0$). Eqn. (16) can then be simplified to

$$\frac{d\omega}{dt} = \frac{\frac{\omega_0}{J_3^p - J_1^p}}{1 - \frac{\omega_0}{J_3^p - J_1^p}\cdot\frac{u_{el}\cdot r_E^2\alpha_0}{\rho_{00}G}}\begin{pmatrix} \left.\frac{dJ_{13}}{dt}\right|_{ve} \\ \left.\frac{dJ_{23}}{dt}\right|_{ve} \\ \frac{4}{3}\left.\frac{dJ_{33}}{dt}\right|_{ve} \end{pmatrix} \tag{17}$$

[*Steinberger*, 1996]. J_3^p and J_1^p are the principal moments of inertia. The third component is approximately zero, since mostly the direction and not the magnitude of ω changes. Eqn. (17) may be trans-

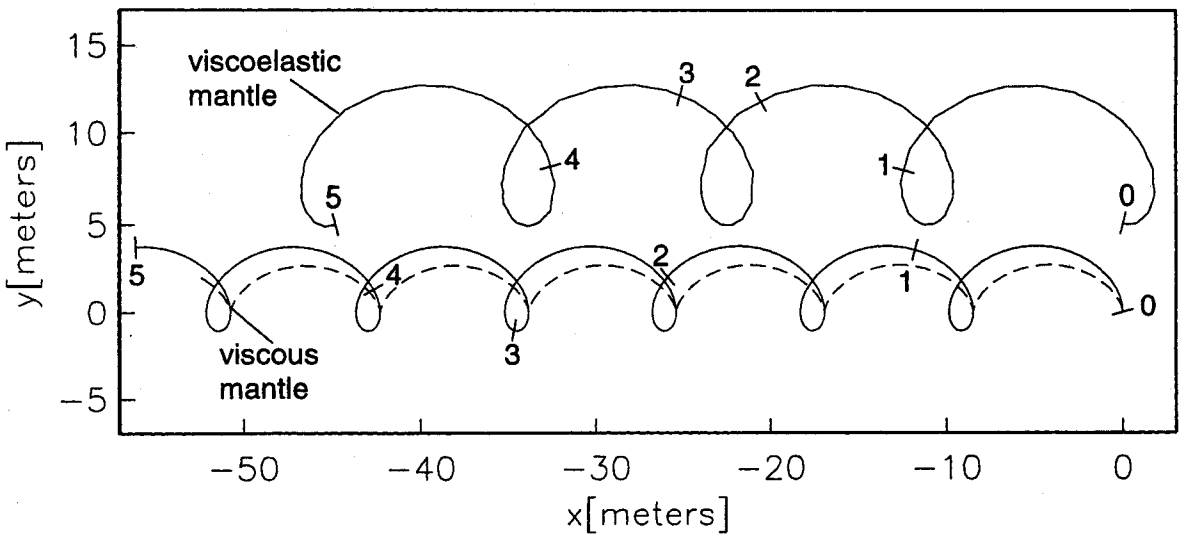

Figure 4. Direct integration of Euler equations over a period of 5 years, showing the Chandler wobble and a secular drift of the pole, due to non-hydrostatic inertia tensor elements $J_{13} = J_{31} = 10^{33}$ kg m^2. Results for a viscous incompressible mantle ($\rho_0 = 4424$ kg m^{-3}) and a core in hydrostatic equilibrium ($\rho_0 = 10\,989$ kg m^{-3}) are contrasted with a result for a viscoelastic mantle (parameters for ρ_0, μ and k as in PREM layer 4 = bulk lower mantle) and a core in hydrostatic equilibrium (ρ_0 as in PREM). $\eta = 6 \cdot 10^{21}$ Pa s in the mantle, $r_{CMB} = 3486$ km, $r_E = 6371$ km in both cases. For better visibility, curves are drawn offset by 5 meters in y direction. Numbers on curves indicate time [in years]. Solid lines: 2 meters initial distance (on Earth surface) between rotation axis and axis of figure; dashed line: zero initial distance.

formed into any other coordinate system. It shows that the immediate elastic deformation has the effect of simply magnifying the rate of change of ω by a factor $\left(1 - \frac{\omega_0}{J_3^p - J_1^p} \cdot \frac{u_{el} \cdot r_E^2 \alpha_0}{\rho_{00} G}\right)^{-1}$, which is a constant number somewhat bigger than 1 for each Earth model and related to the Love numbers. For example, for the PREM Earth model, we calculate a value of 1.485376. Also, it shows that the speed at which the rotation axis changes is directly proportional to the speed of viscoelastic relaxation, which is itself inversely proportional to viscosity: If the viscosity is everywhere increased by a factor n, the speed at which the rotation axis moves will decrease by a factor $1/n$. Unlike the case of direct integration, the rotation vector is now uniquely determined by the shape, therefore the components of the rotation vector are not integrated as independent variables, but were rather calculated from the inertia tensor at each time step.

Figure 5 compares results from direct and quasi-static integrations. The left panel shows that there are virtually no differences in the long-term behavior. This result, which can be reproduced for any viscous Earth model, serves as justification to use henceforth the quasi-static integration. In the viscoelastic case, direct integration is extremely slow with the present algorithm, and was thus not performed for any extended periods of time. The right panel shows that both curves disagree by a few meters after the pole moved by about 150 km. The initial Chandler wobble is damped down to a steady-state magnitude of less than 10 cm with a damping time of about 5000 years. This is a much longer time than the actual damping time of the wobble, indicating that the anelastic effects acting on short timescales are more important causes of damping than viscous effects in the mantle.

Some results of quasi-static integration were presented by *Steinberger and O'Connell* [1997], Figure 3. This figure essentially showed that the speed at which the rotation axis moves is mainly determined by lower mantle viscosity. In this figure, the axis labels of the right panels in the second and third row were misprinted. They should correctly be 6×10^5 and 1.2×10^6. In the caption, the mantle viscosity assumed in the first, second and fourth row, was given incorrectly; it is $6 \cdot 10^{21}$Pas. The fourth row was calculated for a viscous rheology (not viscoelastic, as wrongly written in the caption).

In Figure 6 we compare results of the time domain and the eigenmode approach, for a calculation of vis-

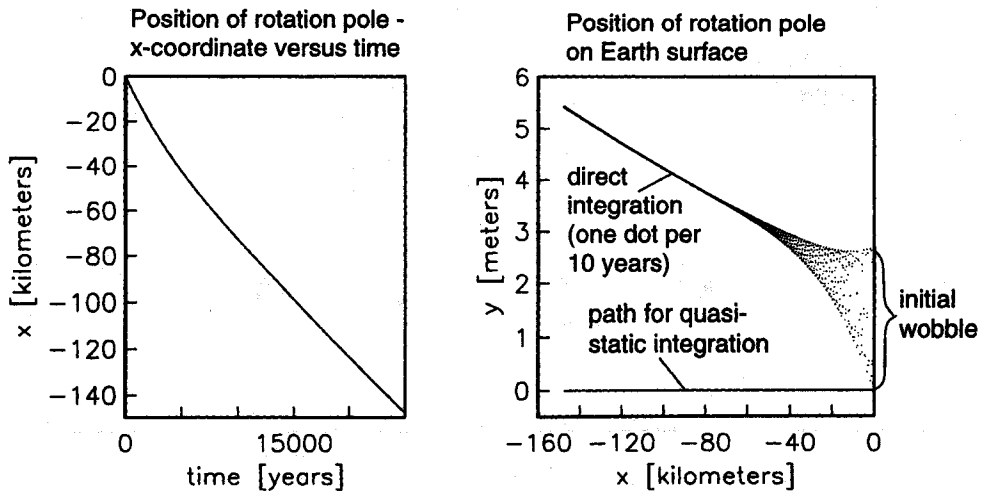

Figure 5. Direct and quasi-static integration of Euler equations over a period of 25 000 years, for a viscous Earth model and excess masses as in Figure 4. In the left panel, the two curves are virtually identical. For the direct integration, the rotation axis is initially coinciding with the axis of figure.

coelastic relaxation towards a new equilibrium shape. For an instantaneous change of the rotation axis of 1 degree, we plot the corresponding non-diagonal inertia tensor element as a function of time. In the eigenmode approach, we fit only radial displacement on chemical boundaries with a density jump (CMB, surface, internal boundaries) using an appropriate number of eigenmodes of viscoelastic decay. For two boundaries (surface and CMB), we use modes M0 and C0, for three boundaries (surface, 670 km, CMB) we use M0, C0, M1. For four boundaries (surface, 400 km, 670 km, CMB) we use M0, C0, M1, M2, neglecting all the other modes. This means, we treat a viscoelastic compressible mantle consisting of adiabatic layers entirely analogous to a viscous mantle, where no other modes occur, with the only difference that we also take the immediate elastic deformation into account. The left panel is for constant elastic parameters throughout the mantle, such that the viscoelastic decay spectrum only consists of discrete lines, whereas in the right panel the elastic parameters vary continuously. In both cases, the curves for time domain and eigenmode approach are in very good agreement. Also, the left and right panel are in most places similar, indicating again that the exact shape of the functions $\mu(r)$ and $k(r)$ has only very minor influence on the viscoelastic decay. In the top panels, the relaxation during the first 10 000 years is shown magnified and on a linear scale, demonstrating that on the left side the two curves are almost indistinguishable (the same would be the case for the dashed or dotted lines), whereas on the right side there is a difference of a few per cent (which would be similar for the dotted lines).

2.5.3. Steady-state solution. As we have seen in the previous section, it is mainly the viscosity structure which determines the speed at which the rotation axis may change. Also, starting from an initial state, after some time a steady state is approached in which the buildup of non-hydrostatic shape is compensated by viscoelastic decay. This is illustrated in Figure 7, which shows the rate of change of the rotation vector as a function of time, normalized by a factor which takes into account that the non-hydrostatic mass anomalies, which are originally at 45°, move to a different latitude in the process. This normalizing factor is approximately 1 for small values ω_2/ω_3. A horizontal line corresponds to steady-state. The figure shows that both for a viscous incompressible mantle with constant density and an adiabatic compressible mantle steady state is approached after approximately the decay time of mode C0 (in this case, a few times 10^4 years). However if there is a chemical boundary with a density jump within the mantle the steady state approximation is less valid on this time scale - the line maintains a finite slope. This is due to the mode M1 with its very long decay time. Also, the figure shows that the steady state is approached faster for a viscous rheology, due to the shorter relaxation times of eigenmodes. The transition from an initial state during which the pole moves faster for a viscous rheology (depicted in Figure 4) to a steady state in which the pole moves faster for the viscoelastic rheology is shown at very short times on the figure.

We outline here an analytical steady-state solution for the speed at which the rotation axis changes for a viscous rheology with layers of constant density. This

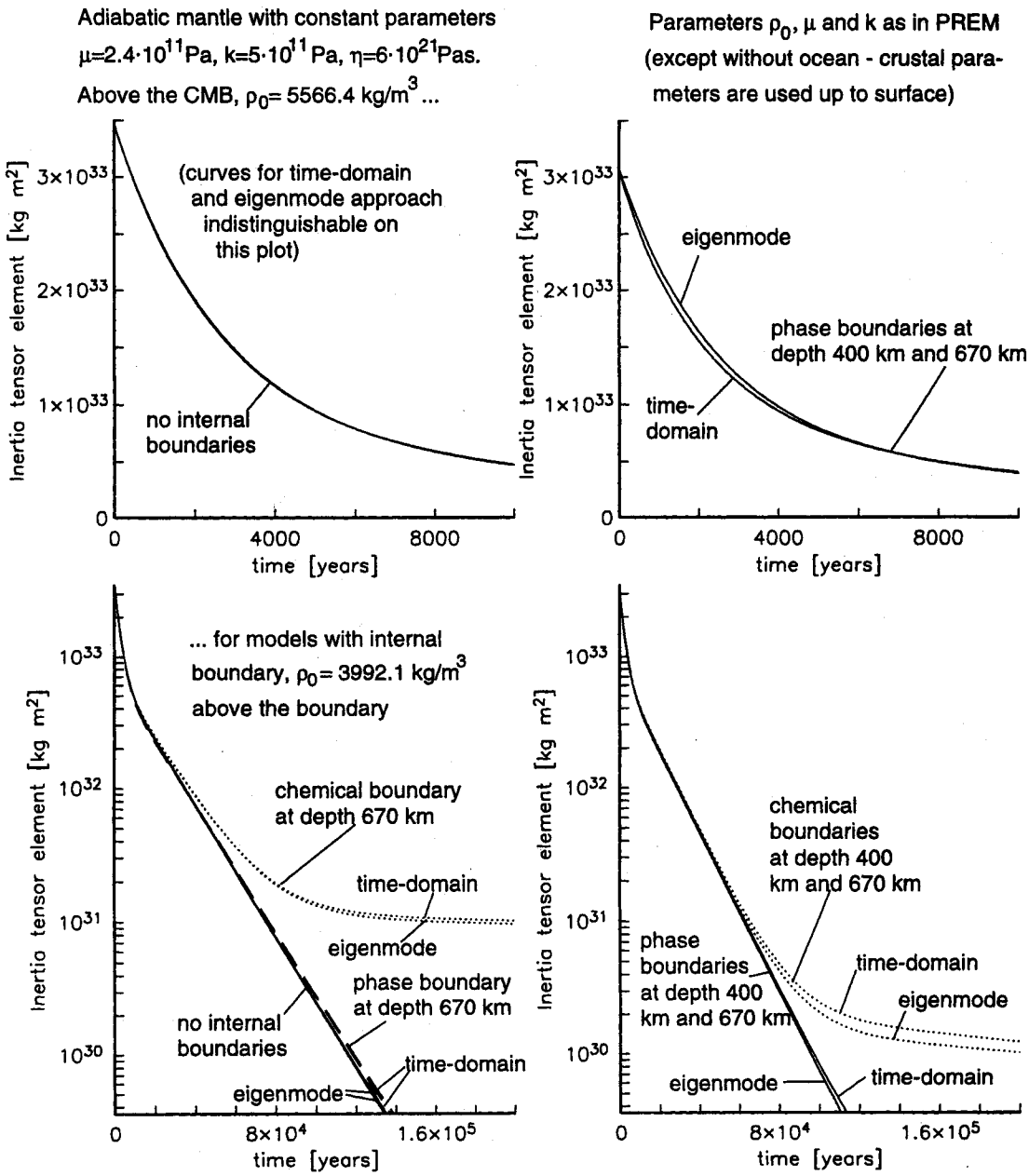

Figure 6. Change of the nondiagonal inertia tensor element due to deformation following an imposed instantaneous change of the rotation axis by 1 degree — comparison of time domain and eigenmode approach for various cases of a viscoelastic mantle and a core (with PREM density structure) in hydrostatic equilibrium. In the top panels, only the continuous lines (for the same models as below) are plotted for better visibility.

solution can also be applied to the eigenmode approximation for a viscoelastic body with adiabatic layers, which was described above, by simply replacing equilibrium radial displacement with equilibrium radial displacement minus radial elastic deformation.

If the rotation axis is parallel to the z-axis, the equilibrium shape is degree two order zero only, and we can express the equilibrium radial displacement $u_{eq}(r_j)$ (w.r.t. spherical symmetry) at radii $r_j, j = 1, \ldots n$ in terms of the radial displacement of the n eigenfunctions of viscous decay $u_i(r_j), i = 1 \ldots n$. r_j are the radii of boundaries with density jumps, e. g. r_1 is the core-mantle-boundary, r_n the surface, and the number of eigenfunctions always matches exactly the number of

boundaries in this case. We can therefore find equilibrium coefficients $c_{i0}, i = 1 \ldots n$ such that

$$u_{eq}(r_j) = c_{i0} u_i(r_j) \omega_0 \tag{18}$$

If the rotation axis changes, a degree two order one component in the spherical harmonic expansion of the equilibrium shape is created. Hence an equal and opposite deviation u_{ne} of the actual shape from equilibrium shape is created. The change in non-equilibrium shape due to this process is

$$\left.\frac{du_{ne}(r_j)}{dt}\right|_1 = -u_i(r_j) c_{i0} \left\{ \begin{array}{ll} \frac{d\omega_x}{dt} & \text{for } Y_{21} \\ \frac{d\omega_y}{dt} & \text{for } Y_{2-1} \end{array} \right\} \tag{19}$$

[*Steinberger*, 1996]. This is compensated by viscoelastic relaxation: The corresponding contribution to the change of the non-equilibrium shape is

$$\left.\frac{du_{ne}(r_j)}{dt}\right|_2 = s_i c_i u_i(r_j) \omega_0 \tag{20}$$

where s_i is the decay constant of mode i, and c_i is the expansion coefficient of the degree two order one part of the actual shape minus equilibrium shape in terms of eigenfunctions, and where, against the usual convention, the summation index i appears three times. Without loss of generality we now assume polar motion in the x-direction. Assuming steady-state we set

$$\left.\frac{du_{ne}(r_j)}{dt}\right|_1 + \left.\frac{du_{ne}(r_j)}{dt}\right|_2 = 0$$

in eqns. (19) and (20), and thus obtain

$$c_{i0} \cdot \frac{d\omega_x}{dt} \cdot \frac{1}{\omega_0} = s_i c_i \tag{21}$$

Furthermore, the rotation axis is always very nearly parallel to the axis of figure. If $J_{13,j}$ is the inertia tensor element corresponding to the j-th eigenfunction and $\mathbf{J}^0$ is the part of the inertia tensor due to initially imposed non-hydrostatic excess masses, this means

$$c_j J_{13,j} + J^0_{13} = 0$$

Using eqn. (21) we can find an expression for the change in ω:

$$\frac{d\omega}{dt} = -\frac{\omega_0 J^0_{13}}{\sum\limits_j c_{j0} J_{13,j}/s_j}. \tag{22}$$

For the cases depicted in Figure 7 we obtain the following values:

viscous rheology		$1.7386 \cdot 10^{-18}$ s^{-2}
viscoelastic rheology	solid line	$1.9427 \cdot 10^{-18}$ s^{-2}
"	dashed line	$2.0307 \cdot 10^{-18}$ s^{-2}
"	dotted line	$1.0486 \cdot 10^{-18}$ s^{-2}

There is good agreement in the first three cases, whereas the agreement is rather poor in the last case. This indicates again that in this case a steady state is not approached over the time scale shown here, because in this case the mode M1 with its very long decay time is present. Once steady state is approached, the speed of polar wander is significantly reduced in the case of a chemical boundary, but before that, results with and without chemical boundary are similar.

The steady-state solution can also be used for a general viscoelastic rheology without the eigenmode approximation, except that the proportionality constant c_{tpw} relating $\frac{d\omega}{dt}$ and $\omega_0 J^0_{13}$ in an equation equivalent to eqn. (22) has to be determined by a numerical integration.

Some results obtained with the steady-state approach for a viscous rheology were already shown by *Steinberger and O'Connell* [1997]. The main conclusion there was that, except for the unusual case of inertial interchange, the rotation axis always follows the axis of the maximum *imposed* non-hydrostatic moment of inertia very closely, unless the viscosity of the lower mantle is much higher than about 10^{23} Pa s (which most researchers would not consider very likely). The results can also be used to estimate the speed of inertial interchange true polar wander: We had shown that, if mass anomalies are emplaced slowly, the maximum rate of polar wander $\left.\frac{d\omega}{dt}\right|_{max} \propto \sqrt{\dot{J}_{13} c_{tpw}}$, whereas for instantaneous emplacement, we obtain $\left.\frac{d\omega}{dt}\right|_{max} \propto J_{13} c_{tpw}$; it is always the slower one of these two rates which is appropriate. For large-scale mantle flow, the first formula is appropriate: for $\dot{J}_{13} = 10^{33}$kg m^2/20Myr and a mantle viscosity $6 \cdot 10^{21}$ Pas, the fourth panel of Figure 3 of that paper had shown a maximum rate of about 30 degrees in 4 Ma. From Figure 2 of that paper, it can be inferred that c_{tpw} is approximately inversely proportional to lower mantle viscosity. If we therefore use the lower mantle viscosity $4 \cdot 10^{22}$ Pas of the viscosity model employed in the next section, and a growth rate $\dot{J}_{13} = 3 \cdot 10^{32}$kg m^2/50Myr which turns out to be a typical value for the models tested in the next section, we obtain a rough estimate for the maximum speed of polar wander driven by mantle convection of about 1 degree per Myr, much slower than inferred in some recent papers [*Kirschvink et al.*, 1997, *Prevot et al.*, 2000, *Sager and Koppers*, 2000].

Numerical models indicate that plume heads may rise significantly faster than typical mantle flow speeds, [*Larsen and Yuen*, 1997, *van Keken*, 1997]. Using the second formula, which is appropriate in this case, and

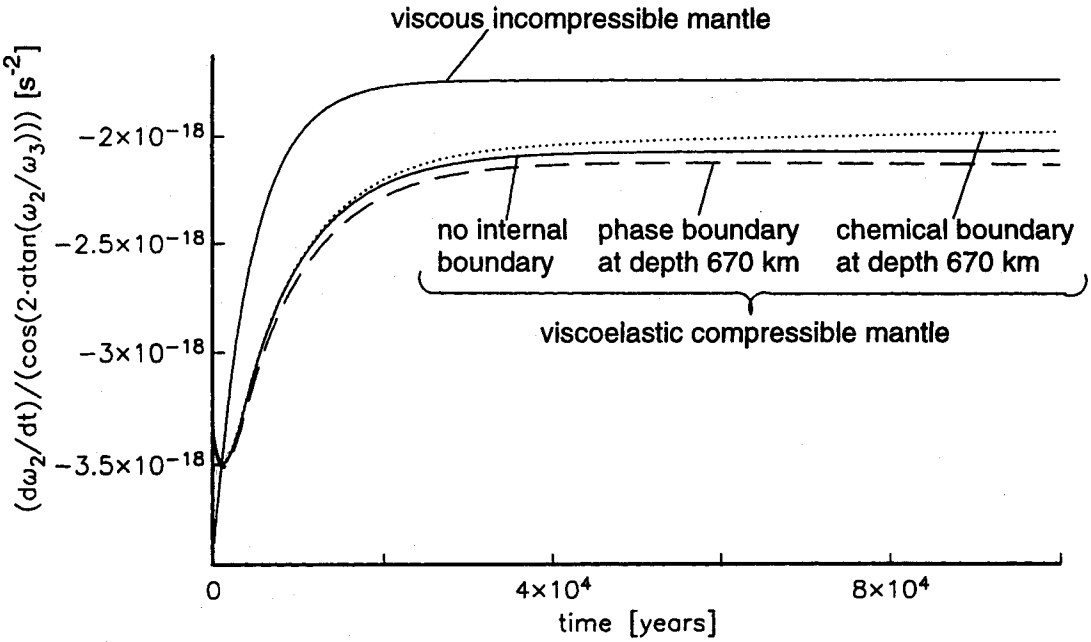

Figure 7. Approach toward steady state for the same models as in the first and second row of *Steinberger and O'Connell* [1997], Figure 3. A horizontal line corresponds to steady state.

reasonable numbers, we find that a fast rising plume-head cannot cause more than a few degrees of true polar wander during the few Ma of its ascent.

3. CHANGE OF AXIS OF MAXIMUM NON-HYDROSTATIC MOMENT OF INERTIA CAUSED BY ADVECTION OF MANTLE DENSITY HETEROGENEITIES

A more realistic distribution of non-hydrostatic mass anomalies than the ones used so far can be inferred from results of seismic tomography. The method of *Hager and O'Connell* [1979, 1981] for calculating flow in a viscous spherical shell, and its extension to calculate the advection of mantle density heterogeneities has been previously explained in detail [*Steinberger and O'Connell*, 1998], and this is not reiterated here. How this method is used to compute true polar wander was outlined by *Steinberger and O'Connell* [1997]. Here we just reiterate a few important points:

- Because the observed geoid is related to the *total* inertia tensor, according to eqn. (12), the degree two order one coefficients of the observed geoid very nearly vanish. This is, however, not the case for the degree two order one coefficients of the geoid calculated from tomographic Earth models, unless we specifically choose scaling factors to convert seismic velocity to density anomalies such as to satisfy this condition. When using a tomographic model to calculate advection of density heterogeneities and corresponding changes of the degree two geoid, we therefore usually add the changes to the *observed* present degree two geoid, rather than the calculated one, in order to calculate the past degree two geoid.
- Although unrealistic, a free upper boundary has been shown to yield the best geoid predictions [*Thoraval and Richards*, 1997]. On the other hand, imposing plate motions as boundary conditions does not yield a good geoid prediction unless layering of the flow is imposed artificially [*Ćadek and Fleitout*, 1999] but we prefer not to do that. Thus, although somewhat inconsistent, we regard it most appropriate to compute changes of the geoid, and hence changes of the rotation axis, by combining geoid kernels that represent a free upper boundary [*Panasyuk et al.*, 1996] with a flow field computed with imposed time-dependent plate motions [*Gordon and Jurdy*, 1986; *Lithgow-Bertelloni et al.*, 1993] as boundary condition.
- We directly compare the paleomagnetic axis with the computed axis of maximum non-hydrostatic moment of inertia, and neglect the difference between *imposed* and *total* non-hydrostatic moment of inertia. This approach is justified as long as

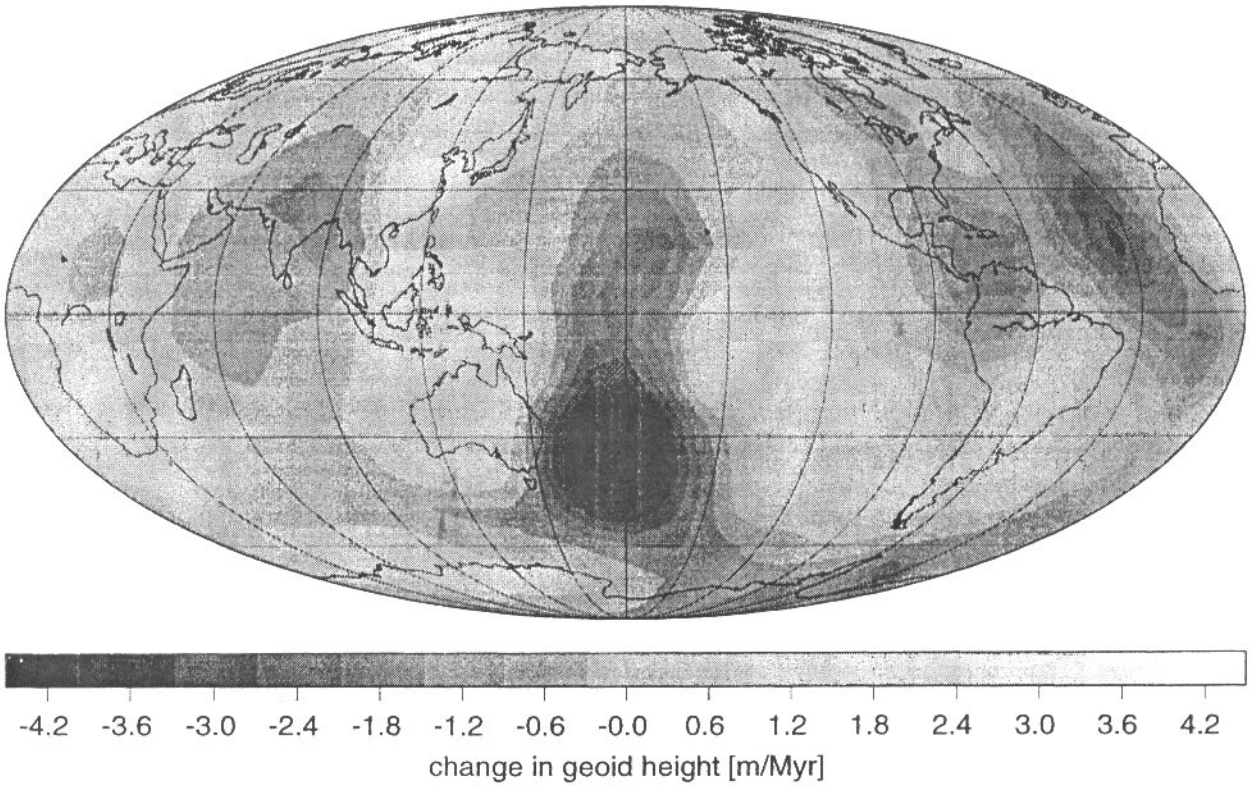

Figure 8. Predicted change of the geoid – degrees 2-12 for the same model as in *Steinberger and O'Connell* [1997], Figure 1. Geoid kernels were computed with a code written by S. V. Panasyuk.

the axis of maximum *imposed* non-hydrostatic moment of inertia moves sufficiently slow (i.e., much slower than the maximum speed of polar wander, estimated in the previous section to be about 1 degree per Myr). The paleomagnetic results indicate that this was the case at least during the Tertiary.

All calculations are done for a compressible mantle with no phase boundaries. All flow fields are expanded up to spherical harmonic degree and order 31. Figure 8 shows the predicted present-day geoid change for the same model of true polar wander shown by *Steinberger and O'Connell* [1997]. It appears that sinking of the geoid centered at the northern tip of New Zealand that is predicted here is the feature most responsible for predicted Cenozoic polar wander towards Greenland: The pole moves such as to maximize the moment of inertia tensor. If the time scale over which mass redistributions occur are sufficiently slow, this means polar motion tends to move regions of sinking geoid to the poles and regions of rising geoid towards the equator. For the comparatively fast mass redistributions associated with recent glaciations however, the delay of the response cannot be neglected: At present the pole is moving towards Hudson Bay, where a large ice mass melted, and hence the geoid was sinking about 20,000 years ago, but is currently rising due to post-glacial rebound. When caused by mantle flow, a sinking of the geoid can result from either the sinking of dense material or the rising of material of low density in a region where the geoid kernel decreases with depth (here, the mid-mantle). In the case of this model, it is a combination of both effects: downgoing cold material apparently related to subduction of the Tonga slab, and an upwelling in the neighboring Pacific. However not all the tomographic models tested lead to this prominent feature of the predicted geoid change.

Figure 9 compares the computed true polar wander for another model with recent paleomagnetic true polar wander curves. These do not start at the present pole, because even for very recent times, the computed paleomagnetic pole is offset from the present pole. The implied recent fast polar motion is most likely due to

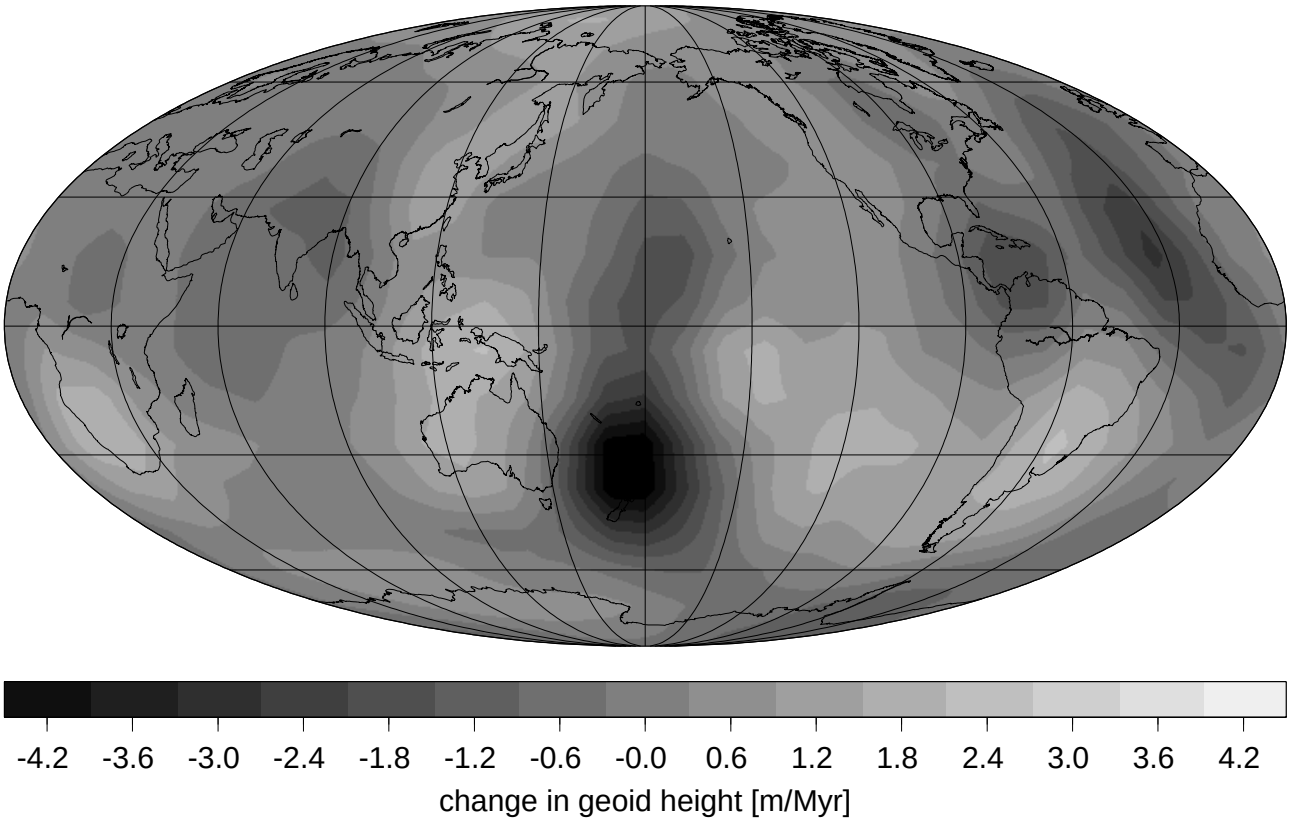
-4.2
-3.6
-3.0
-2.4
-1.8
-1.2
-0.6
-0.0
0.6
1.2
1.8
2.4
3.0
3.6
4.2
change in geoid height [m/Myr]

Figure 8:

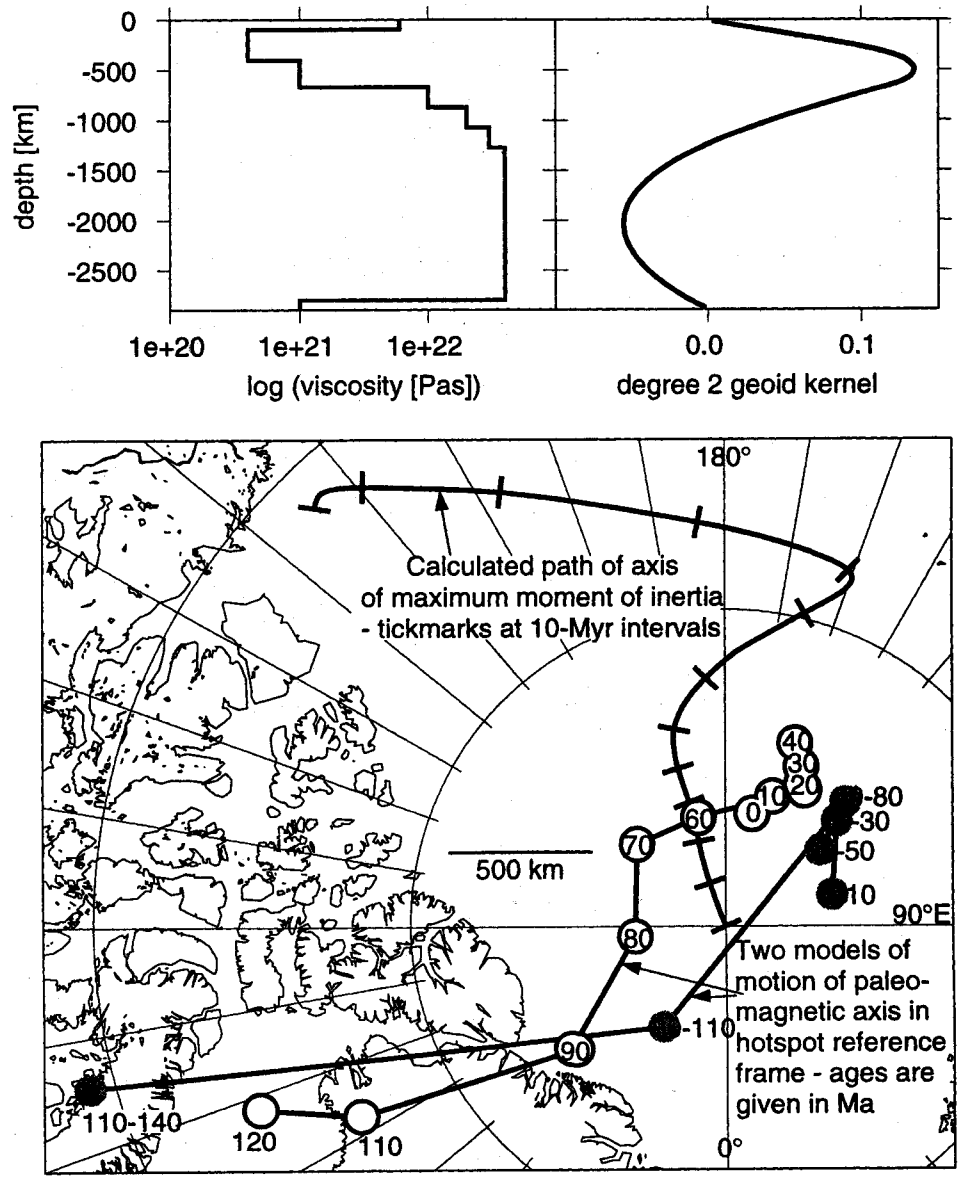

Figure 9. True polar wander – geodynamic calculations and paleomagnetic results. The calculation is done for the viscosity model shown; the degree 2 geoid kernel was computed with a code written by S. V. Panasyuk. Mantle density anomalies below 220 km are inferred from the latest model of *Grand* [2001; pers. comm], (similar to *Grand et al.* [1997]; available via anonymous ftp amazon.geo.utexas.edu), using a conversion factor from seismic velocity to density anomalies $(\delta\rho/\rho) / (\delta v_s/v_s) = 0.3$. Density variations above 220 km depth are disregarded. Paleomagnetic results are from *Besse and Courtillot* [2000; pers. comm.] (black circles) and *Prevot et al.* [2000] (grey dots).

glacial effects, which are not modelled here. The two paleomagnetic results shown here and our modelling agree in two aspects:

- Slow polar motion of only a few degrees during the Tertiary roughly towards Greenwich.
- Faster polar motion prior to that. This faster motion ends at around 60 Ma and changes direction at around 80 Ma in our geodynamic model, and it ends at 50 or 80 Ma according to the paleomagnetic results. The direction of faster polar motion prior to about 80 Ma predicted from the geody-

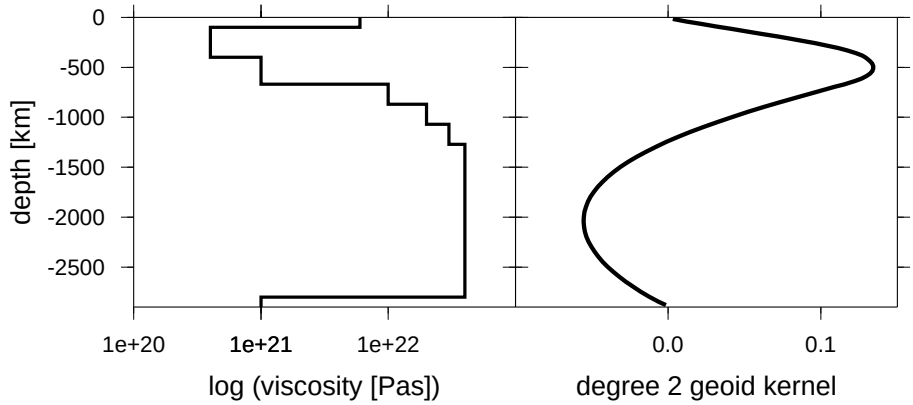
0
-500
-1000
-1500
-2000
-2500
depth [km]
1e+20
1e+21
1e+22
log (viscosity [Pas])
0.0
0.1
degree 2 geoid kernel

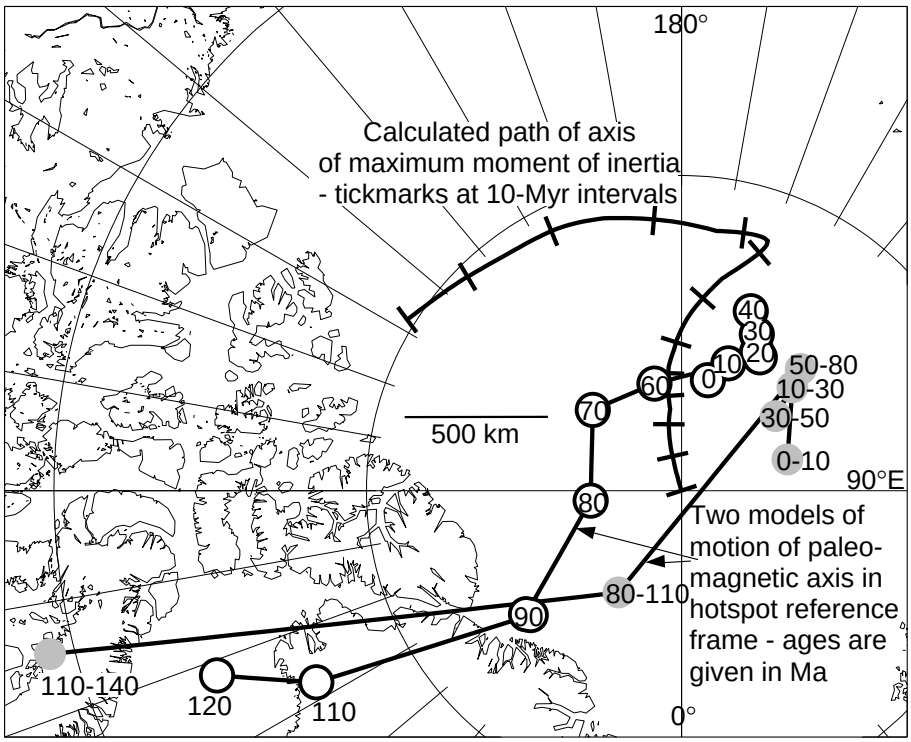
180°
Calculated path of axis
of maximum moment of inertia
- tickmarks at 10-Myr intervals
500 km
40
30
20
10
0
60
70
80
90
80-110
50-80
10-30
30-50
0-10
90°E
Two models of
motion of paleo-
magnetic axis in
hotspot reference
frame - ages are
given in Ma
110-140
120
110
0°

Figure 9:

namic model differs by about 30 degrees from the average direction inferred from paleomagnetism.

Such a result was however only obtained for this particular model. Figure 10 shows results for a larger number of tomographic models: For a constant conversion factor below 220 km (solid circles) the models all predict similar direction and magnitude of polar motion. One problem with such predictions is, of course, that we are not able to adequately predict the present-day geoid, unless we modify viscosity structure and/or conversion factors from seismic velocity to density anomalies $(\delta\rho/\rho)\,/\,(\delta v_s/v_s)$ separately for each model. Particularly, matching the non-hydrostatic excess flattening of the Earth is a problem, which has been previously discussed by *Forte et al.* [1993, 1995]. A better match can be obtained by choosing a particular viscosity profile, but at the expense of deteriorating the fit to other geoid coefficients. Here we include some results where we modify the conversion factors only within reasonable bounds (Table 1) such that $J_{13} = 0$ and $J_{23} = 0$ and the polar axis is actually the predicted rotation axis. This is only done for those three models, for which the predicted axis of figure is already within 15 degrees of the rotation axis for a constant $(\delta\rho/\rho)\,/\,(\delta v_s/v_s) = 0.2$ below 220 km depth. For the light shaded dots, we then still adjust the remaining non-zero inertia tensor elements, for the dark shaded dots no further adjustments are done. Obviously this is a very preliminary approach, but it shows that directions of polar motion stay broadly similar, regardless of the procedure taken. For the dark shaded dots, faster polar wander is predicted, because here the predicted differences between the polar and equatorial non-hydrostatic moments of inertia are much smaller than observed, in agreement with the results of *Forte et al.*, [1993]. These results indicate that the procedure of adding the difference between predicted and observed moments of inertia does not fundamentally undermine our results.

4. DISCUSSION

We have developed a formalism for viscoelastic relaxation combined with the Liouville equations to calculate changes in the rotation axis. Calculations were done for a very simple non-hydrostatic mass distribution, consisting of only two positive and two negative excess masses. This assumed mass distribution (no dynamic compensation, no sinking) is far simpler and less realistic than previously assumed by others [e.g., *Spada et al.*, 1992, *Ricard et al.*, 1993], but it still contains the essential physics of true polar wander and makes results more easily comprehensible, we believe. A direct integration with no further approximations was compared with a "quasi-static" approximation, where the rotation axis is assumed to be always exactly parallel to the axis of maximum moment of inertia, leading to almost indistinguishable results. An even simpler steady-state solution was derived. This solution may be used over timescales longer than the decay time of the slowest-decaying mode. For an adiabatic mantle, this will be around 10,000 – 100,000 years (depending on viscosity), for an internal chemical boundary, it may be more than a million years.

Since our approach is independent of previous work, benchmark comparisons would be important, but would require a more dedicated effort: Our results obtained so far cannot be directly compared with results of true polar wander due to glacial effects, such as compiled by *Mitrovica and Milne* [1998], because of the different loading history: Whereas these results were obtained for a "saw-tooth" loading history to mimic the effect of repeated glaciations, we use an instantaneously imposed constant mass load, or a linear increase of loading. Also, these models usually contain an elastic lithosphere, which is not included in our models. The most successful predictions of the geoid due to mantle flow use a viscous lithosphere, with viscosity intermediate between the low-viscosity upper mantle and the high-viscosity lower mantle, and a free upper boundary [e.g., *Thoraval and Richards*, 1997]. We therefore regard that, with more realistic models of the lithosphere with lateral variations only beginning to emerge, this is also most appropriate for modelling true polar wander on the timescales of mantle convection. The lithosphere will then not play an important role in determining rates of polar wander and is hence completely neglected here. We will qualitatively compare our results with those compiled by *Mitrovica and Milne* [1998] for a high deep mantle viscosity $\gtrsim 10^{22}$ Pas, because in this case, the elastic lithosphere will play a less important role: E.g. comparison of models a, b, c and d of *Ricard et al.*, [1992], Table 2 shows that in the case of an isoviscous mantle with 10^{21} Pas, the presence of a lithosphere increases decay times of modes M0 and C0 by factors 3.8 and 2.4, whereas for a lower mantle viscosity of $3 \cdot 10^{22}$ Pas, the M0 relaxation time remains the same and the C0 relaxation time increases by a factor of 1.6. Hence in the second case, the presence of the lithosphere will reduce polar wander speed by a much smaller amount than in the first case. A direct comparison is also difficult with published results that account for dynamic compensation and partly use a more

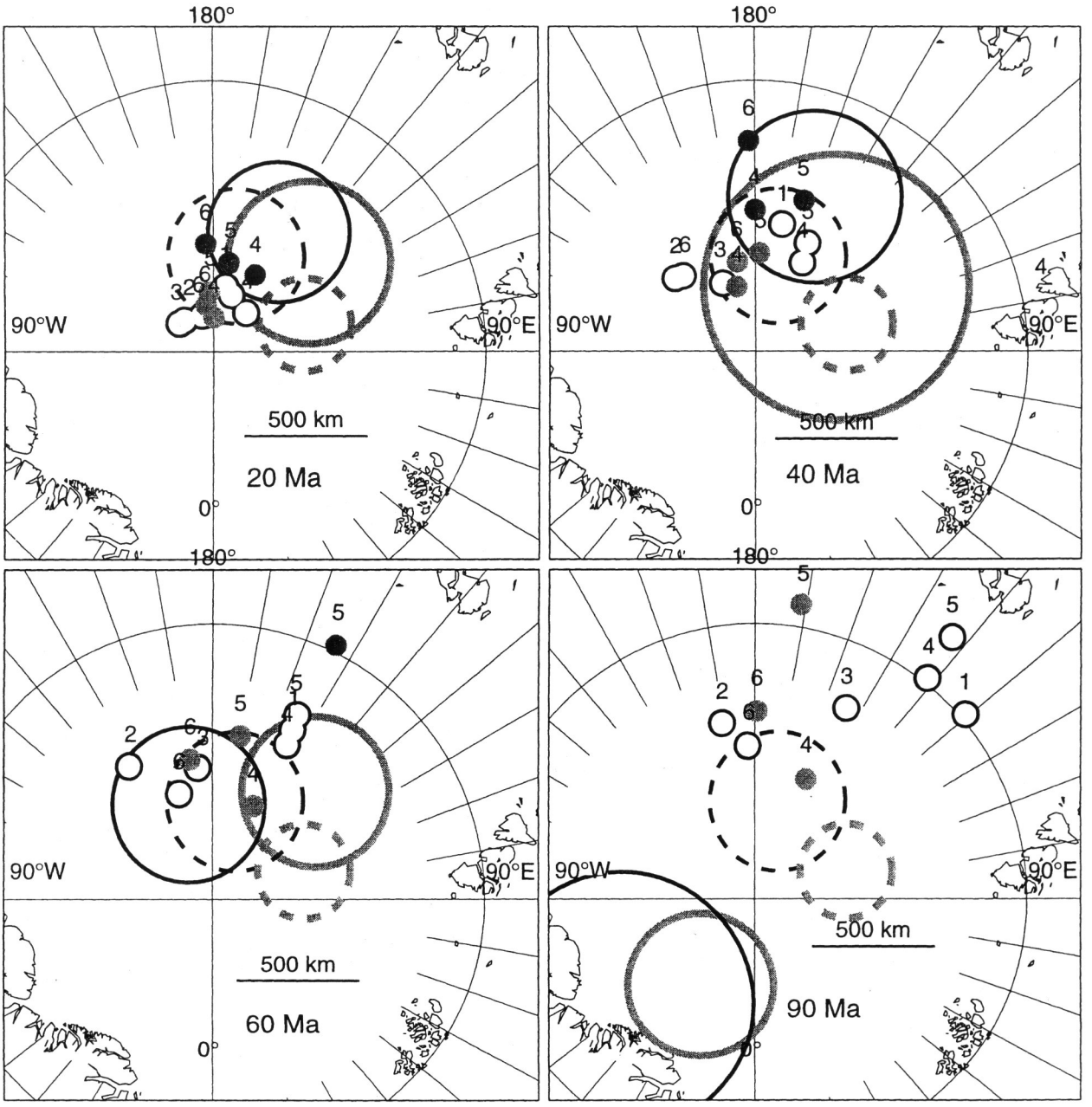

Figure 10. Pole positions at 20, 40, 60 and 90 Ma – geodynamic calculations and paleomagnetic results. Calculations are done for the viscosity model shown in Figure 9 using various tomographic models to infer mantle density. The models are indicated by numbers: 1 = S12WM13 *Su et al.* [1994]; 2 = S20A *Ekström and Dziewonski* [1998], isotropic part; 3 = S20RTS *Ritsema and Van Heijst* [2000], 4 = SAW24B16 *Mégnin and Romanowicz* [2000], 5 = SB4L18 *Masters et al.* [2000], 6 = latest model *Grand* [2001; pers. comm]; Positions indicated by solid circles are calculated for a constant $(\delta\rho/\rho)\,/\,(\delta v_s/v_s) = 0.2$ below 220 km depth; Positions indicated by light and dark shaded filled circles are calculated for a conversion factor varying with depth, as listed in Table 1, such that predicted geoid coefficients C_{21} and S_{21} vanish. The difference between actual and calculated present-day degree-two geoid coefficients is added for solid circles and light shaded filled circles; no adjustments are done for dark shaded filled circles. Density variations above 220 km depth are disregarded. Paleomagnetic results are from *Besse and Courtillot* [2000; pers. comm.] (large solid circles) and *Prevot et al.* [2000] (large shaded circles). Continuous circles show the pole position at the respective time, with circle radius equal to the 95% confidence interval A_{95}, dashed circles show the pole position for the most recent time interval.

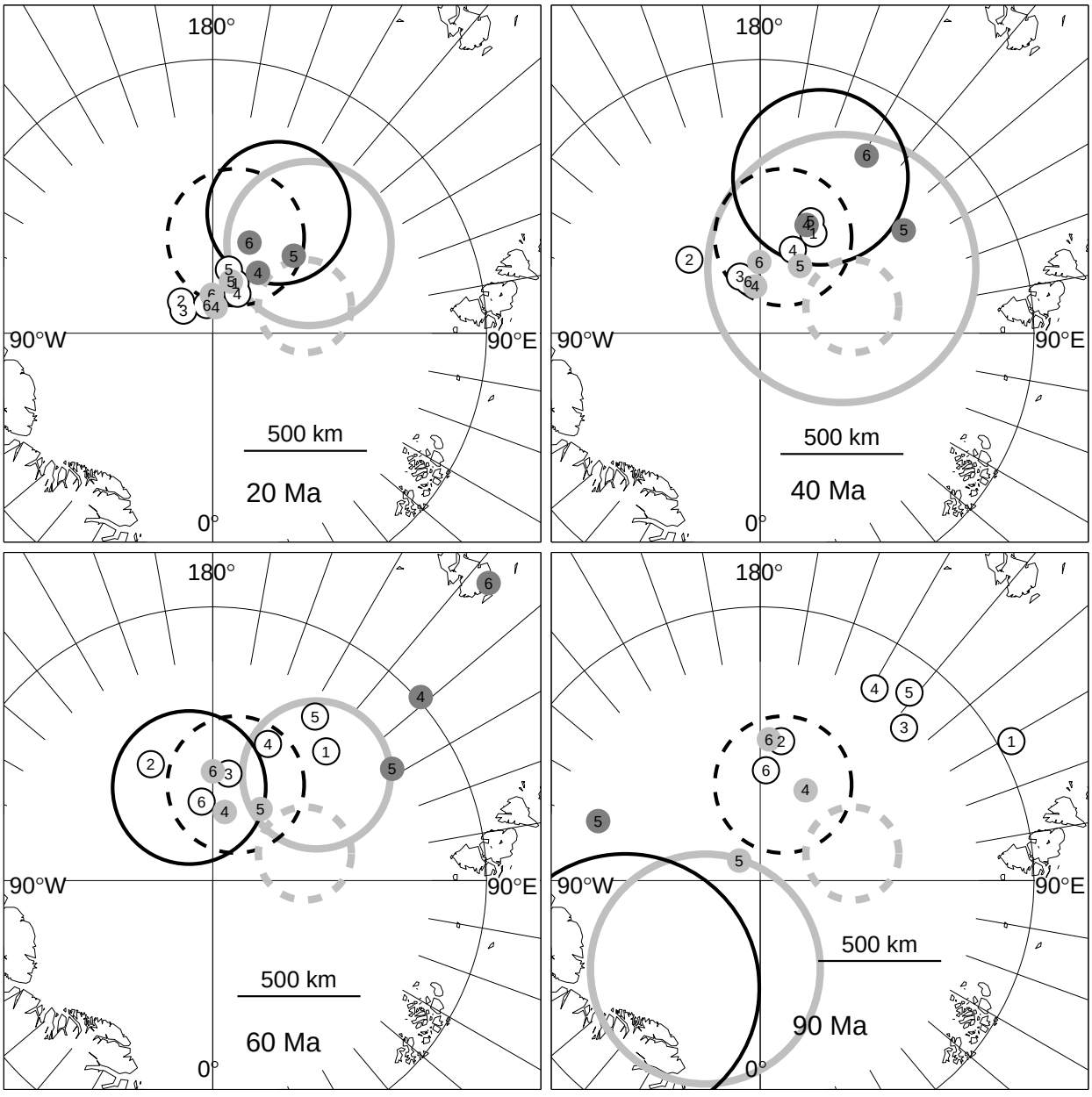
180°
90°W
90°E
0°
500 km
20 Ma
180°
90°W
90°E
0°
500 km
40 Ma
180°
90°W
90°E
0°
500 km
60 Ma
180°
90°W
90°E
0°
500 km
90 Ma

Figure 10:

Table 1. Conversion factors $(\delta\rho/\rho)\,/\,(\delta v_s/v_s)$ used for computing the shaded filled circles in Figure 10, for different depth intervals and tomographic models.

Model	Grand	SB4L18	SAW24B16
220 km to 410 km	0.29	0.17	0.10
410 km to 670 km	0.28	0.00	0.00
670 km to d_{lm}	0.25	0.20	0.20
d_{lm} to 2900 km	0.15	0.30	0.32
d_{lm}	2600 km	1800 km	2600 km

complicated time-dependent loading history [*Spada et al.*, 1992, *Ricard et al.*, 1992, 1993, *Vermeersen et al.*, 1996] e.g. to model true polar wander driven by subduction. Some other works on long-term polar [*Sabadini and Yuen*, 1989, *Ricard and Sabadini*, 1990] permit a more quantitative comparison, however because of differences in the density and elastic structure of the models, exact agreement with published results cannot be expected either. With that in mind, we compare various aspects of our results with other publications:

- Effects of compressibility on rates of polar wander: From eqn. (17) we see that any difference between viscous incompressible and viscoelastic compressible Earth models is a composite of two effects: The increase of polar wander speed due to immediate elastic deformation (about 50 % for the PREM Earth model), and differences in the slow viscous or viscoelastic rate of change of the inertia tensor in both cases. The two effects can counteract, and for the models shown in Fig. 7 with no internal boundary, the polar wander speed is still faster by about 20 % for the viscoelastic Earth model in the case of steady state, whereas it is about 10 % slower in Fig. 2 of *Mitrovica and Milne* [1998], for a high deep-mantle viscosity, and can be several tens of % slower according to *Vermeersen et al.* [1996].

- Rates of polar wander and deep mantle viscosity: Our results [*Steinberger and O'Connell*, 1997, Fig. 2, left panel, solid line] can be re-scaled to an upper mantle viscosity 10^{21} Pas (equals 10^{22} P) and then converted to the rotational excitation factor A_1 defined by *Sabadini and Yuen* [1989]. Our model then yields $A_1 \approx 0.15\text{kyr}^{-1}$ for a lower mantle viscosity $\eta_{lm} = 10^{22}$ Pas and $A_1 \approx 0.029\text{kyr}^{-1}$ for $\eta_{lm} = 10^{23}$ Pas, whereas we read from *Ricard and Sabadini*, 1990, Fig. 4 corresponding values $A_1 \approx 0.13\text{kyr}^{-1}$ and $\approx 0.017\text{kyr}^{-1}$. Given their description, we conclude that *Sabadini and Yuen* [1989] wrongly labelled their curves and that the continuous one is without chemical boundary, and hence to be compared with. Under that assumption we read corresponding values of $A_1 \approx 0.15\text{kyr}^{-1}$ and $\approx 0.019\text{kyr}^{-1}$ from their Fig. 1. We attribute our somewhat faster rates to the absence of an elastic lithosphere, which significantly increases the decay times of modes M0 and C0, and thus slows polar wander [*Ricard et al.*, 1992]. Also the shape of the curves is somewhat similar: A_1 is roughly inversely proportional to η_{lm} for η_{lm} between 10^{21} and 10^{22} Pas, and the curves become somewhat flatter for larger η_{lm}. However, *Sabadini and Yuen* [1989] show a flattening for $\eta_{lm} > 10^{23}$ Pas, whereas our curve already becomes flatter above 10^{22} Pas.

- Rates of polar wander and the thickness of a high-viscosity layer in the deep mantle: In our model, the speed of polar wander is roughly inversely proportional to the thickness of a high-viscosity layer in the lower mantle [*Steinberger and O'Connell*, 1997, Fig. 2, right panel]. For a high viscosity below 1400 km, the polar wander speed should therefore be increased by about one third compared to a high viscosity in the entire mantle below 670 km. *Mitrovica and Milne* [1998] (Fig. 3) also show that their results are quite similar regardless of the depth of the viscosity boundary, but that *Peltier and Jiang* [1996] obtain polar wander speeds that differ by orders of magnitude for the two cases.

- Effect of a chemical boundary on rates of polar wander: Our results indicate that before steady-state is reached, the rates of polar motion with and without chemical boundary are similar, but in steady-state a chemical boundary can significantly reduce speed of polar motion. For the models shown here, it is reduced by about a factor of two, whereas in the corresponding models (with constant mantle viscosity) shown by *Saba-*

dini and Yuen [1989], Fig. 1 and *Ricard and Sabadini* [1990] Fig. 4 it is reduced by a factor ≈ 3.5 and ≈ 5.5 respectively. This reduction is due to the presence of the mode M1 with its long relaxation time. If we re-scale our model shown in Fig. 3 to a viscosity of 10^{21} Pas and hence divide relaxation times by 6, we find a M1 relaxation time of 241 kyr, almost the same as *Ricard et al.* [1992], for the corresponding model e of their Table 2. This table also shows that the M1 relaxation time gets several times longer if an elastic lithosphere is added to the model, thus the effect of the chemical boundary on rates of polar wander is stronger in the models with elastic lithosphere. The effect of a chemical boundary on rates of polar wander is further discussed by *Mitrovica and Milne* [1998].

In agreement with results obtained by others, our results show that the rotational equations can be accurately integrated in an effective manner, and computational limitations do not pose a problem. While the mechanism of true polar wander can hence be considered well understood, and numerical methods for its computation well developed, the actual true polar wander of the Earth and its relation to the Earth's geodynamic evolution remain poorly known and controversial. A better understanding of actual true polar wander is not merely of academic interest, as it may be linked to other issues, such as the evolution of life on Earth, as e.g. proposed by *Kirschvink et al.* [1997].

Here we have shown geodynamic models of true polar wander for a number of tomographic models. They generally agree on a polar motion of the order of 5 degrees during the past 60 Ma roughly towards Greenwich, which is not in conflict with paleomagnetic results. In order to compute such a slow polar motion in roughly such a direction, a degree two geoid kernel that reverses sign with roughly equal magnitude on either side is required. Such a geoid kernel is also needed to successfully explain the present-day geoid. Calculations for viscosity structures which yield qualitatively different geoid kernels yield polar motions too large to be consistent with the observations. If a larger conversion factor from seismic velocity to density is assumed, an increased magnitude of polar motion results, but the direction stays more or less the same.

For the viscosity structure adopted here, the computed recent polar motion due to mantle convection typically amounts to about 10 % of that observed geodetically, but if the viscosity of the lower mantle is $\leq 10^{22}$ Pa s, it may be up to about 40 % [*Steinberger and O'Connell*, 1997]. Based on the figures shown by *Mitrovica and Milne* [1998], and references cited therein, a 10-20 % decrease of polar wander rate due to glacial effects may quite drastically change inferences on deep mantle viscosity. On the other hand, mantle flow contribution to rotational variations $\dot{J}_2$ computed from the same models typically turn out to be well below 1 % of the observed rate, i.e. there is no significant effect.

Prior to about 60 Ma, the computations apparently become less reliable and the differences between our various geodynamic model results increase. Only for the tomographic model of *Grand*, [2001, pers. comm.], a faster polar motion in a direction similar to what is inferred from paleomagnetism was computed. This geodynamic model predicts true polar wander speeds of not more than about 0.5 degrees per Myr. The paleomagnetic results disagree on the speed of polar motion: Whereas *Besse and Courtillot* [2000, pers. comm.] report speeds of no more than about 0.5 degrees per Myr, i.e. well below our estimated "speed limit" of about 1 degree per Myr, *Prevot et al.* [2000] obtain higher speeds exceeding 5 degrees per Myr around 80 Ma. *Sager and Koppers* [2000] use Pacific data and obtain 3–10 degrees per Myr around 84 Ma, however these results have been questioned by *Tarduno and Smirnov* [2001] and *Cottrell and Tarduno* [2000]. Our estimated speed limit is of course not a stringent bound, since we cannot exclude that mantle convection has been more vigorous and mantle viscosity lower than in our model at some time in the past, however this is unlikely during the last 100 Myrs.

A possibly even faster true polar wander event earlier in Earth history has been proposed by *Kirschvink et al.*, [1997], but questioned by *Torsvik et al.*, [1998]. It is presently not possible to set up an actualistic model of an event so far back in time – over timescales longer than ≈ 100 Ma models of subduction history as well as the advection of mantle density heterogeneities become unreliable, and a different approach has to be used: *Richards et al.* [1999] therefore combine mantle convection models with the rotational dynamics described by *Ricard et al.* [1993]. While this approach does not allow to model the actual true polar wander further back into the past, it can yield insight into questions such as which properties an Earth model must have such that the frequencies of "inertial interchanges" (i.e. that the maximum and intermediate non-hydrostatic principal moments of inertia become equal) are close to what is observed (i.e. not more than once every few hundred Myr).

We anticipate that better constraints on both mantle density anomalies and mantle viscosity will give more reliable predictions of true polar wander in the near fu-

ture. Tomographic models are now beginning to agree on their large-scale features, and we have shown here that a number of models generally yield similar predictions of true polar wander. The "observed" true polar wander that dynamic model predictions are compared to is also becoming more reliably constrained. Besides paleomagnetic data, sea level variations have recently been proposed as an observable to detect true polar wander [*Mound and Mitrovica*, 1998], particularly for events of inertial interchange true polar wander [*Mound et al.*, 1999].

Furthermore we expect that it will be possible to explain parts of tomographic anomalies in terms of subduction history in a dynamically consistent model. This should give better constraints on mantle viscosity and also facilitate a comparison between true polar wander predictions from tomography (as done here) and from subduction history [*Richards et al.*, 1997] and hence also to better assess the effect of dynamic upwellings on true polar wander. In this way, input parameters to convection models and their (in a statistical sense) predicted true polar wander [*Richards et al.*, 1999] will also become better constrained.

Acknowledgments. We like to thank Ming Fang and Bert Vermeersen for discussions about viscoelastic relaxation, Svetlana Panasyuk for a routine to compute geoid kernels, all the authors of the models used for supplying their models, especially Steve Grand for his latest yet unpublished tomographic model, and Jean Besse for his latest yet unpublished true polar wander model. Reviews by Giorgio Spada and Jerry X. Mitrovica helped to clarify a number of points, and especially put this work in the context of previous publications. This work was partially supported by NSF grants EAR-9205930 and EAR-9814666.

REFERENCES

Alterman, Z. H., H. Jarosch, and C. L. Pekeris, Oscillations of the earth, *Proc R. Soc. London, Ser. A, 252*, 80-95, 1959.

Andrews, J. A., True polar wander: An analysis of Cenozoic and Mesozoic paleomagnetic poles, *J. Geophys. Res., 90*, 7737-7750, 1985.

Besse, J., and V. Courtillot, Revised and synthetic apparent polar wander paths of the African, Eurasian, North American and Indian plates, and true polar wander since 200 Ma, *J. Geophys. Res., 96*, 4029-4050, 1991.

Boschi, L., J. Tromp and R. J. O'Connell, On Maxwell singularities in postglacial rebound, *Geophys. J. Int., 136*, 492-498, 1999.

Burgers, J., Rotational motion of a sphere subject to viscoelastic deformation, 1, 2, 3, *Konikl. Ned. Akad. Wetenschap. Proc., 58*, 219-237, 1955.

Čadek, O., and L. Fleitout, A global geoid model with imposed plate velocities and partial layering. *J. Geophys. Res., 104*, 29055-29075, 1999.

Clairaut, M., Théorie de la figure de la terre, tirée des principes de l'hydrostatique, Paris, *Ches David fils*, 1743.

Cottrell, R. D., and J. A. Tarduno, Late Cretaceous true polar wander: not so fast, *Science, 288*, www.sciencemag.org/cgi/content/full/288/5475/2283a, 2000.

Darwin, G., On the influence of geological changes on the earth's axis of rotation, *Phil. Trans. Roy. Soc. London, A, 167*, 271-312, 1877.

Dickman, S. R., Secular trends in the Earth's rotation pole: Consideration of the motion of latitude observatories, *Geophys. J. R. Astron. Soc., 51*, 229-244, 1977.

Duncan, R. A., N. Petersen, and R. B. Hargraves, Mantle plumes, movement of the European plate and polar wandering, *Nature, 239*, 82, 1972.

Dziewonski, A. M., and D. L. Anderson: Preliminary Reference Earth Model, *Phys. Earth Planet. Inter., 25*, 297-356, 1981.

Ekström, G., and A. M. Dziewonski, The unique anisotropy of the Pacific upper mantle, *Nature, 394* 168-172, 1998.

Fang, M., and B. H. Hager, The singularity mystery associated with a radially inhomogeneous Maxwell viscoelastic structure, *Geophys. J. Int., 123*, 849-865, 1995.

Forte, A. M., A. M. Dziewonski, and R. L. Woodward, Aspherical structure of the mantle, tectonic plate motions, nonhydrostatic geoid, and topography of the core-mantle boundary, in *Dynamics of the Earth's Deep Interior and Earth Rotation, Geophys. Monogr. Ser., 72*, edited by J.-L. Le Mouël, D. E. Smylie, and T. Herring, pp. 135-166, AGU, Washington, D. C., 1993.

Forte, A. M., J. X. Mitrovica, and R. L. Woodward, Seismic-geodynamic determination of the origin of excess ellipticity of the core-mantle boundary, *Geophys. Res. Lett., 22*, 1013-1016, 1995.

Gold, T., Instability of the earth's axis of rotation, *Nature, 175*, 526-529, 1955.

Goldreich, P., and A. Toomre, Some remarks on polar wandering. *J. Geophys. Res., 74*, 2555-2569, 1969.

Gordon, R. G, and D. M. Jurdy, Cenozoic global plate motions, *J. Geophys. Res., 91*, 12389-12406, 1986.

Gordon, R.G. and R. A. Livermore, Apparent polar wander of the mean lithosphere reference frame, *Geophys. J. R. astr. Soc., 91*, 1049-1057, 1987.

Grand, S. P., R. D. Van der Hilst, and S. Widiyantoro, Global seismic tomography: A snapshot of convection in the Earth, *GSA Today, 7*, 1-7, 1997.

Gurnis, M., J. X. Mitrovica, J. Ritsema, and H.-J. van Heijst, Constraining mantle density structure using geological evidence of surface uplift rates: The case of the African superplume, *Geochem., Geophys., Geosys., 1*, 1999GC000035, 2000.

Hager, B. H., and R. J. O'Connell, Kinematic models of large-scale mantle flow, *J. Geophys. Res., 84*, 1031-1048, 1979.

Hager, B. H., and R. J. O'Connell: A simple global model of plate dynamics and mantle convection, *J. Geophys. Res., 86*, 4843-4867, 1981.

Han, D., and J. Wahr, The viscoelastic relaxation of a realistically stratified Earth, and a further analysis of postglacial rebound, *Geophys. J. Int., 120*, 287-311, 1995.

Hanyk, L., J. Moser, D. A. Yuen, and C. Matyska, Time-domain approach for the transient responses in stratified

viscoelastic Earth models, *Geophys. Res. Lett., 22*, 1285-1288, 1995.

Hargraves, R. B., and R. A. Duncan, Does the mantle roll? *Nature, 245*, 361-363, 1973.

Inglis, D., Shifting of the earth's axis of rotation, *Rev. Mod. Phys, 29*, 9-19, 1957.

Jeffreys, H., *The Earth*, Cambridge University Press, New York, 1952.

Jurdy, D., and R. Van der Voo, A method for the separation of true polar wander and continental drift including results for the last 55 m.y., *J. Geophys. Res., 79*, 2945-2952, 1974.

Jurdy, D., True polar wander, *Tectonophysics, 74*, 1-16, 1981.

Kirschvink, J. L., R. L. Ripperdan, and D. A. Evans, Evidence for a large-scale reorganization of Early Cambrian continental masses by inertial interchange true polar wander, *Science, 277*, 541-545, 1997.

Lambert, W., F. Schlesinger, and E. Brown, The variation of latitude, *Bull. 78 U.S. Nat. Res. Coun., 16*, 245, 1931.

Larsen, T. B., and D. A. Yuen, Fast plumeheads: Temperature-dependent versus non-Newtonian rheology, *Geophys. Res. Lett., 24*, 1995-1998, 1997.

Lithgow-Bertelloni, C., M. A. Richards, Y. Ricard, R. J. O'Connell, and D. C. Engebretson, Toroidal-poloidal partitioning of plate motions since 120 ma, *Geophys. Res. Lett., 20*, 375-378, 1993.

Livermore, R. A., F. J. Vine, and A. G. Smith, Plate motions and the geomagnetic field, II, Jurassic to Tertiary, *Geophys. J. R. Astron. Soc., 79*, 939-961, 1984.

Masters, G., G. Laske, H. Bolton, and A. Dziewonski, The relative behavior of shear velocity, bulk sound speed, and compressional velocity in the mantle: implications for chemical and thermal structure, in *Seismology and Mineral Physics, Geophys. Monogr. Ser., 117*, edited by S. Karato, pp. 63-87, AGU, Washington, D. C., 2000.

McElhinny, M. W., Mantle plumes, paleomagnetism and polar wandering, *Nature, 241*, 523, 1973.

Mégnin, C., and B. Romanowicz, The shear velocity structure of the mantle from the inversion of of body, surface and higher modes waveforms, *Geophys. J. Int, 143*, 709-728, 2000.

Mitrovica, J. X., and G. A. Milne, Glacial-induced perturbations in the Earth's rotation: A new appraisal, *J. Geophys. Res., 103*, 985-1005, 1998.

Mound, J. E., and J. X. Mitrovica, True polar wander as a mechanism for second-order sea-level variations, *Science, 279*, 534-537, 1998.

Mound, J. E. , J. X. Mitrovica, D. A. D. Evans, and J. L. Kirschvink, A sea-level test for inertial interchange true polar wander events, *Geophys. J. Int, 136*, F5-F10, 1999.

Munk, W., Polar wandering: a marathon of errors, *Nature, 177*, 551-554, 1956.

Munk, W., and G. J. F. MacDonald, *The Rotation of the Earth*, Cambridge University Press, New York, 1960.

Panasyuk, S. V., B. H. Hager, and A. M. Forte, Understanding the effects of mantle compressibility on geoid kernels, *Geophys. J. Int., 124*, 121-133, 1996.

Peltier, W. R., Glacial-isostatic adjustment – II. The inverse problem, *Geophys. J. R. astr. Soc., 46*, 669-705, 1976.

Peltier, W. R., and X. Jiang, Glacial isostatic adjustment and Earth rotation: Refined constraints on the viscosity of the deepest mantle, *J. Geophys. Res., 101*, 3269-3290, 1996.

Prevot, M., P. Camps, and M. Daignières, Evidence for a 20° tilting of the Earth's rotation axis 110 million years ago, *Earth Planet. Sci. Lett, 179*, 517-528, 2000.

Ricard, Y., and R. Sabadini, Rotational instabilities of the Earth induced by mantle density anomalies, *Geophy. Res. Lett., 17*, 627-630, 1990.

Ricard, Y., R. Sabadini, and G. Spada, Isostatic deformations and polar wander induced by redistribution of mass within the Earth, *J. Geophys. Res., 97*, 14223-14236, 1992.

Ricard, Y., G. Spada, and R. Sabadini, Polar Wandering on a dynamic Earth, *Geophys. J. Int., 113*, 284-298, 1993.

Richards, M. A., Y. Ricard, C. Lithgow-Bertelloni, G. Spada, and R. Sabadini, An explanation for Earth's long-term rotational stability *Science, 275*, 372-375, 1997.

Richards, M. A., H.-P. Bunge, Y. Ricard, and J. R. Baumgardner, Polar Wandering in mantle convection models, *Geophys. Res. Lett., 26*, 1777-1780, 1999.

Ritsema, J., and H. J. Van Heijst, Seismic imaging of structural heterogeneity in Earth's mantle: Evidence for large-scale mantle flow, *Science Progress, 83 (3)* 243-259, 2000.

Sabadini, R. D., D. A. Yuen, and E. Boschi, Polar wander and the forced responses of a rotating, multilayered, viscoelastic planet, *J. Geophys. Res., 87*, 2885-2903, 1982.

Sabadini, R., D. A. Yuen, and E. Boschi, A comparison of the complete and truncated versions of the polar wander equations *J. Geophys. Res., 89* 7609-7620, 1984.

Sabadini, R., and D. A. Yuen, Mantle stratification and long-term polar wander, *Nature, 339*, 373-375, 1989.

Sager, W. W., and A. A. P. Koppers, Late Cretaceous polar wander of the Pacific plate: Evidence of a rapid true polar wander event, *Science, 287*, 455-459, 2000.

Spada, G., Y. Ricard, and R. Sabadini, Excitation of true polar wander by subduction, *Nature, 360*, 452-454, 1992.

Spada, G., R. Sabadini, and E. Boschi, The spin and inertia of Venus, *Geophys. Res. Lett., 23*, 1997-2000, 1996a.

Spada, G., R. Sabadini, and E. Boschi, Long-term rotation and mantle dynamics of the Earth, Mars and Venus, *J. Geophys. Res., 101*, 2253-2266, 1996b.

Steinberger, B. M., Motion of hotspots and changes of the Earth's rotation axis caused by a convecting mantle, Ph.D. thesis, 203 pp., Harvard Univ., Cambridge, Mass., Jan. 1996.

Steinberger, B., and R. J. O'Connell, Changes of the Earth's rotation axis owing to advection of mantle density heterogeneities, *Nature, 387*, 169-173, 1997.

Steinberger, B., and R. J. O'Connell, Advection of plumes in mantle flow: Implications for hotspot motion, mantle viscosity and plume distribution, *Geophys. J. Int., 132*, 412-434, 1998.

Steinberger, B., and R. J. O'Connell, Effects of mantle flow on hotspot motion, in *The History and Dynamics of Global Plate Motions, Geophys. Monogr. Ser., 121*, edited by M. A. Richards, R. G. Gordon, and R. D. van der Hilst, pp. 377-398, AGU, Washington, D. C., 2000.

Steinberger, B., Plumes in a convecting mantle: Models and observations for individual hotspots, *J. Geophys. Res., 105*, 11,127–11,152, 2000.

Tarduno, J. A., and A. V. Smirnov, Stability of the Earth with respect to the spin axis for the last 130 million years, *Earth Planet. Sci. Lett., 184*, 549-553, 2001.

Thoraval, C., and M. A. Richards, The geoid constraint in global geodynamics: viscosity structure, mantle heterogeneity models and boundary conditions, *Geophys. J. Int., 131*, 1-8, 1997.

Torsvik, T. H., J. G. Meert, and M. A. Smethurst, Polar wander and the Cambrian, *Science, 279*, www.sciencemag.org/cgi/content/full/279/5347/9a, 1998.

Su, W., R.L. Woodward, and A. M. Dziewonski, Degree 12 model of shear velocity heterogeneity in the mantle, *J. Geophys. Res., 99*, 6945-6980, 1994.

van Keken, P., Evolution of starting mantle plumes: A comparison between numerical and laboratory models, *Earth Planet. Sci. Lett., 148*, 1-11, 1997.

Vermeersen, L. L. A., R. Sabadini, and G. Spada, Compressible rotational deformation, *Geophys. J. Int., 126*, 735-761, 1996.

Wu, P., and W. R. Peltier, Pleistocene glaciation and the Earth's rotation: A new analysis, *Geophys. J. R. astr. Soc., 76*, 753-791, 1984.

B. Steinberger, Institut für Meteorologie und Geophysik, Johann Wolfgang Goethe-Universität, Feldbergstr. 47 60323 Frankfurt am Main, Germany. (e-mail: steinber@geophysik.uni-frankfurt.de

R. J. O'Connell, Department of Earth and Planetary Sciences, Harvard University 20 Oxford Street, Cambridge, MA 02138.
(e-mail: oconnell@geophysics.harvard.edu)